MASTERARBEIT | MASTER'S THESIS

Titel | Title

Biological functions of OEF18 – a novel Calcium binding protein located in peroxisomes and chloroplasts

verfasst von | submitted by

Jannik van Werde B.Sc.

angestrebter akademischer Grad | in partial fulfilment of the requirements for the degree of

Master of Science (MSc)

Wien | Vienna, 2024

Studienkennzahl lt. Studienblatt | Degree programme code as it appears on the student record sheet:	UA 066 865
Studienrichtung lt. Studienblatt | Degree programme as it appears on the student record sheet:	Masterstudium Molecular Biology
Betreut von | Supervisor:	Dipl.-Chem. Dr. Markus Teige

Acknoledgements

I would like to thank my supervisor Dr. Markus Teige for offering me the OEF18 project. Your advice, encouragement, and suggestions for improvement have been invaluable. I am especially grateful for the opportunity to work in your group prior to my Master's thesis.

I would like to sincerely thank Dr. Bernhard Wurzinger and Dr. Bushra Ijaz for the invaluable support in the lab and the introduction of molecular biology techniques, advice and suggestions. Thank you very much for the great work with you.
Also, many thanks to Dr. Przemyslaw Kmiecik for providing the OEF18 lines, Figure 1 and 2 and offering me help with background questions on OEF18 from his previous experiments,

Many thanks to Prof. Andreas Bachmair for providing the yeast strain for the Y2H assay and for providing the positive control. Many thanks to Jose Julián Valenzuela for providing the sCherry vector and many thanks to Marintia Nava for the atg5 knockout mutant.

Many thanks also to the entire Bachmair group. Thank you so much fall all the advices on my endless questions. It was a really great time working with you guys.

I would like to point out that in this scientific work artificial intelligence was used as a tool to support text processing, whereby scientific accuracy and personal contribution were always in the foreground. The result was checked by the author.

Lastly, I would like to thank my parents, my girlfriend and her family. Thank you for motivating me to keep going and not give up.

Table of Contents

Abstract

Plants are immobile organisms and cannot escape unfavorable environmental conditions. To cope with such stresses, various mechanisms have been evolved that allow them to detect environmental signals and adjust their metabolism accordingly. One of the key organelles involved in plant adaptation to environmental changes is the chloroplast. As the site of photosynthesis, chloroplasts are not only crucial for energy production but also act as sensors and mediators of stress responses. One potential sensor is the EF-hand protein OEF18 (Organellar EF-hand protein, 18 kDa), identified by Dr. Simon Stael and biochemically characterized by Dr. Przemyslaw Kmiecik. OEF18 is localized in both the outer chloroplast envelope and the membrane of peroxisomes, and it binds calcium ions under physiological conditions through its cytoplasm-facing EF-hand domain. However, its exact biological function has remained unknown.

This Master's thesis demonstrates the involvement of OEF18 in chloroplast stromule formation in *Arabidopsis thaliana* under normal conditions, and also highlights a role for calcium ions in this process. However, when stromule formation was induced by the addition of sucrose, OEF18 showed no effect. Moreover, the *oef18/oef18l* double knockout line displayed no phenotype under various stress conditions that induce autophagy, such as starvation, high light, or heat stress, thereby largely excluding a role for OEF18 in chlorophagy. Additionally, no involvement of OEF18 in the degradation of transitory starch in chloroplasts could be demonstrated, contradicting the previous findings by Dr. Kmiecik, which now appear to be outliers. The potential interaction between OEF18 and microtubules was also intriguing, as Dr. Kmiecik observed this in unbiased protein-protein interaction experiments. It is already known that microtubules play a crucial role in stromule formation in *Nicotiana benthamiana*. However, a targeted yeast two-hybrid assay to verify the interaction between OEF18 and microtubules was inconclusive, as the positive control, along with all other constructs, failed to grow.

In summary, these data suggest that OEF18 is involved in chloroplast stromule formation in *A. thaliana* under normal conditions, with calcium ions playing an additional role in this process. However, OEF18 does not appear to be directly involved in chlorophagy, and its interaction with microtubules remains uncertain.

Zusammenfassung

Pflanzen sind unbewegliche Organismen und können daher unerwünschten Umweltbedingungen nicht entkommen. Um dennoch auf verschiedenste Stressfaktoren reagieren zu können, haben sich im Laufe der Zeit verschiedene Mechanismen entwickelt, die es ermöglichen, Signale zu erkennen und ihren Stoffwechsel entsprechend anzupassen. Eine zentrale Rolle bei der Anpassung an Umweltveränderungen spielt der Chloroplast. Als Ort der Photosynthese ist er nicht nur für die Energieproduktion entscheidend, sondern auch als Sensor und Vermittler von Stressreaktionen aktiv. Ein solcher potenzieller Sensor ist das EF-Hand-Protein OEF18 (organellares EF-Hand-Protein, 18 kDa), das von Dr. Simon Stael identifiziert und von Dr. Przemyslaw Kmiecik biochemisch charakterisiert wurde. OEF18 ist sowohl in der äußeren Chloroplastenhülle als auch in der Peroxisomenmembran lokalisiert und bindet unter physiologischen Bedingungen Kalzium-Ionen. Seine genaue biologische Funktion war bisher unbekannt.

In dieser Masterarbeit konnte die Beteiligung von OEF18 an der Bildung von Chloroplasten-Stromuli in *Arabidopsis thaliana* unter Kontrollbedingungen nachgewiesen werden. Zudem gibt es Hinweise auf eine Rolle von Kalzium in diesem Prozess. Bei stromuleinduzierenden Bedingungen, wie der Zugabe von Saccharose, zeigte OEF18 hingegen keine Wirkung. Da die *oef18/oef18l*-Doppel-Knockout-Linie unter verschiedenen Stressbedingungen, welche Autophagie auslösen (wie Nährstoffmangel, starkes Licht oder Hitzestress), keinen auffälligen Phänotyp aufwies, kann eine Beteiligung von OEF18 an Chlorophagie-Prozessen weitgehend ausgeschlossen werden. Eine Rolle von OEF18 beim Abbau von transitorischer Stärke im Chloroplasten konnte ebenfalls nicht bestätigt werden, was die vorherigen Ergebnisse von Dr. Kmiecik infrage stellt, die möglicherweise auf einen Ausreißer hindeuten.

Von Interesse war außerdem die potenzielle Interaktion von OEF18 mit Mikrotubuli, die Dr. Kmiecik in unvoreingenommenen Protein-Protein-Interaktionsexperimenten beobachtete. Es ist bereits bekannt, dass Mikrotubuli eine wichtige Rolle bei der Bildung von Stromuli in *Nicotiana benthamiana* spielen, die genaue Rolle in Arabidopsis ist jedoch noch unklar. Der gezielte Yeast-two-hybrid Test zur Untersuchung der Interaktion von OEF18 mit β-Tubulinen konnte jedoch aufgrund eines Versagens der Positivkontrolle nicht bestätigt werden.

Zusammenfassend legen diese Ergebnisse nahe, dass OEF18 unter normalen Bedingungen an der Stromulibildung in *A. thaliana* beteiligt ist und dabei Kalzium eine unterstützende Rolle spielt. Eine direkte Beteiligung von OEF18 an Chlorophagieprozessen konnte hingegen weitgehend ausgeschlossen werden. Die Interaktion mit Mikrotubuli bleibt bisweilen unklar.

1 Introduction

Plants are sessile and accordingly, they are exposed to changing environmental conditions reaching from lack of energy sources, pathogen attack or physical damage. Because they cannot move to a less problematic environment unlike animals, they have to deal with their environment, and for that a complex signaling system to react specifically on even the tiniest changes has been evolved. This system is composed of various protein kinases, metabolic substrates and other secondary messengers as well as transcription factors, to mediate plant metabolism to ensure survival under stress conditions.

One of the key organelles that plays a central role in plant adaptation to environmental changes is the chloroplast. As the site of photosynthesis, chloroplasts are not only crucial for energy production but also act as sensors and mediators of various stress responses. When plants face conditions such as light fluctuations, nutrient deprivation, or oxidative stress, chloroplasts can undergo dynamic changes in their structure and function. For instance, they may form thin, tubular extensions known as stromules (stroma-filled tubules extending from plastids), which are thought to facilitate inter-organellar communication and stress signaling. However, under more extreme conditions where damage to the chloroplast is irreversible, the plant must remove these dysfunctional organelles to prevent cellular harm. This degradation process, which is vital for maintaining cellular homeostasis and responding to stress, is orchestrated by autophagy. In the context of chloroplasts, this process is known as chlorophagy—a selective form of autophagy responsible for recycling damaged or surplus chloroplasts, ensuring the plant can efficiently manage its resources and survive under adverse conditions. Understanding autophagy and its role in chloroplast turnover is therefore crucial for grasping how plants regulate their internal machinery in response to stress (Yagyu and Yoshimoto, 2024; Bassham *et al.*, 2006; Hanson and Hines, 2018).

Autophagy, derived from the Greek words meaning "self-eating," is a highly conserved process across all eukaryotes, underscoring its fundamental importance across different organisms. Various types of autophagy have been identified, including macroautophagy, microautophagy, megaautophagy, and chaperone-mediated autophagy (Mizushima and Komatsu, 2011; Das *et al.*, 2012; Avin-Wittenberg, 2018). In plants, organelle-specific autophagy plays a crucial role, particularly in the removal of damaged or unnecessary organelles like chloroplasts (chlorophagy), peroxisomes (pexophagy), and mitochondria (mitophagy), enabling plants to

maintain cellular health and adapt to environmental stressors (Yagyu and Yoshimoto, 2024; Bassham *et al.*, 2006; Ohsumi, 2014).

Macroautophagy

Macroautophagy, often simply referred to as autophagy, is a highly conserved catabolic process across eukaryotic cells, including plants. In this process, cytoplasmic components, such as organelles, are enclosed in double-membrane vesicles called autophagosomes. These vesicles then merge with lysosomes or vacuoles, where their contents are broken down and reused (Veljanovski and Batoko, 2014). In plants, macroautophagy is crucial in preserving cellular balance, to respond to environmental stress, and regulating energy resources when nutrients are limited (Yagyu and Yoshimoto, 2024; Zeng *et al.*, 2024). The autophagy key components can be divided into several groups/complexes:

Core ATG proteins (autophagy related proteins), including ATG1, ATG8, ATG12, and ATG13, play central roles in the regulation, formation, and function of autophagosomes. Their interactions and modifications, such as phosphorylation and lipidation, are critical for autophagosome dynamics. The PI3K (phosphoinosite-3-kinase) complex, including vacuolar protein sorting (VPS)34 and ATG6, is essential for the generation of Phosphatidylinositol 3-phosphate (PI3P), which recruits downstream ATG proteins to the site of autophagosome formation. SNAREs (N-ethylmaleimide-sensitive-factor attachment receptor), for instance Vesicle-associated membrane protein7 (VAMP7), play a role in facilitating the fusion of autophagsomes with the vacuole, allowing the degradation of cargo (Díaz-Troya *et al.*, 2008; Bassham *et al.*, 2006; Doelling *et al.*, 2002; Zhuang *et al.*, 2016).

The activation of macroautophagy in plants is primarily regulated by the Target of Rapamycin (TOR) kinase pathway, which is highly conserved across eukaryotes. Under nutrient-rich conditions, TOR kinase is active and inhibits autophagy by phosphorylating key ATG proteins. Conversely, under nutrient starvation or stress conditions, TOR is inactivated, leading to the dephosphorylation of those key ATG proteins and the induction of autophagy (Wang *et al.*, 2021). The initiation of macroautophagy involves the assembly of the ATG1 kinase complex, which includes ATG1, ATG13, and ATG17 in yeast, and their plant homologs, such as ATG1 and ATG13. This complex is then recruited to the phagophore assembly site (PAS), where it interacts with other ATG proteins to initiate the formation of the isolation membrane, which is also known as the phagophore (Kamada *et al.*, 2000; Bassham *et al.*, 2006). The nucleation

step involves the activation of the class III PI3K complex I, which includes VPS34, VPS15, ATG6 (Beclin1 in mammals), and ATG14 (Su *et al.*, 2020; Kihara *et al.*, 2001). This complex is responsible for the production of phosphatidylinositol 3-phosphate (PI3P) on the nascent phagophore membrane, which serves as a platform for the recruitment of other ATG proteins necessary for autophagosome formation. Phagophore expansion is driven by two ubiquitin-like conjugation systems. The first system involves the conjugation of ATG12 to ATG5, facilitated by ATG7 and ATG10 (Bassham *et al.*, 2006; Yagyu and Yoshimoto, 2024). The ATG12-ATG5 conjugate then interacts with ATG16 to form the ATG12-ATG5-ATG16 complex, which acts as an E3-like enzyme to facilitate the second conjugation system (Romanov *et al.*, 2012). The second system involves the conjugation of ATG8 (LC3 in mammals) to phosphatidylethanolamine (PE), mediated by ATG4, ATG7 and ATG3. The lipidation of ATG8-PE is crucial for the elongation of the phagophore and the formation of the autophagosome. ATG8-PE also plays a key role in cargo recognition and autophagosome maturation by interacting with autophagy receptors such as NBR1, which bind to ubiquitinated cargos (Michaeli *et al.*, 2016). While macroautophagy can be non-selective, such as engulfing bulk cytoplasm during starvation, it can also be selective, by targeting specific organelles or protein aggregates for degradation. This selectivity is mediated by receptor proteins such as NBR1, which recognize ubiquitinated substrates and interact with ATG8 via the ATG8 interacting motif (AIM) on the autophagosome membrane (Svenning *et al.*, 2011). This selective autophagy is critical for the degradation of damaged mitochondria (mitophagy), peroxisomes (pexophagy), and chloroplasts (chlorophagy). Following phagophore elongation, the edges of the membrane close to form a complete autophagosome, encapsulating the cytoplasmic material targeted for degradation. This step involves membrane fusion events mediated by SNARE proteins, which facilitate the final sealing of the autophagosome (Svenning *et al.*, 2011; Johansen and Lamark, 2011).

The mature autophagosome then fuses with the vacuole, the plant equivalent of the lysosome in animal cells. This fusion procedure releases the autophagic body into the vacuolar lumen, where it is degraded by vacuolar hydrolases (Zhang *et al.*, 2020). The breakdown products, such as amino acids, lipids, and sugars, are then recycled end transported back into the cytoplasm for reuse by the cell (Bassham, 2009; Soto-Burgos *et al.*, 2018) .

Macroautophagy plays a crucial role in plant survival, particularly during periods of nutrient deprivation. When resources are rare, plants rely on macroautophagy to degrade cellular

components and release essential nutrients, enabling them to sustain vital processes . Additionally, to nutrient deprivation, plants are frequently exposed to various environmental stresses such as heat or drought, salinity, and pathogen attack (Bassham, 2007). Macroautophagy helps mitigate these stresses by selectively removing damaged organelles, proteins, and other cellular components that could otherwise accumulate and lead to cellular dysfunction or death. This protective mechanism is essential for maintaining cellular homeostasis and ensuring plant survival under adverse conditions (Yagyu and Yoshimoto, 2024). Beyond its role in stress responses, macroautophagy is also involved in several developmental processes. For instance, during leaf senescence, macroautophagy contributes to the degradation of chloroplasts and other organelles, facilitating the remobilization of nutrients to other parts of the plant where they are needed for growth and development (Hörtensteiner and Feller, 2002). Similarly, macroautophagy plays a role in seed germination and the transition from vegetative to reproductive growth, where it helps optimize the allocation of resources to support these critical phases of the plant life cycle (Yagyu and Yoshimoto, 2024; Liu and Bassham, 2012).

Microautophagy

Microautophagy operates through the invagination, protrusion, or septation of the lysosomal or vacuolar membrane to sequester cytoplasmic cargo (De Duve and Wattiaux, 1966). In plants, this process occurs primarily in the vacuole. As in Macroautophagy the engulfed material is eventually degraded by hydrolytic enzymes present within the vacuole, allowing the cell to recycle the basic building blocks like amino acids and lipids (Yagyu and Yoshimoto, 2024).

The initiation of microautophagy in plants is likely being triggered by cellular stress conditions such as nutrient deprivation, oxidative stress, or damage to cellular components. The regulatory pathways involved are still under investigation, but they may also involve the Target of Rapamycin (TOR) signaling pathway (Sieńko *et al.*, 2020).

Membrane dynamics in microautophagy involeves the vacuolar membrane which undergoes invagination or protrusion under the influence of autophagic signaling to engulf cytoplasmic components. The membrane then pinches off the invaginated portion, encapsulating the cytoplasmic material into vesicles inside the vacuole. This process requires a coordinated

action of various proteins, some of which are homologous to those involved in macroautophagy (Zhuang and Jiang, 2019).

The ESCRT (Endosomal Sorting Complex Required for Transport) machinery is a critical player in the membrane remodeling events required for microautophagy. In yeast and mammals, ESCRT complexes mediate membrane scission events during microautophagy, and similar roles are suggested in plants. The ESCRT complexes (ESCRT-0, -I, -II, and -III) function sequentially to recognize, sequester, and expel membrane-bound vesicles containing the cargo for degradation (Schuck et al., 2014).

In addition to the ESCRT machinery, Rab GTPases and SNARE proteins are involved in the fusion of vesicles with the vacuolar membrane. Rab GTPases regulates various steps of vesicular trafficking, including the docking and fusion of microautophagic vesicles. SNARE proteins facilitate the final fusion of the vesicle with the vacuolar membrane, ensuring the transport of the cargo into the vacuole for degradation (Yagyu and Yoshimoto, 2024).

While ATG proteins are more directly associated with macroautophagy, some may also play a role in microautophagy, particularly those involved in membrane dynamics. For instance, ATG8 which is involved in the formation of autophagosomes in macroautophagy, has been implicated in the recognition and sequestration of cargo in microautophagy (Bassham, 2009).

Recent studies have begun to elucidate the role of ATG proteins in microautophagy. For example, anthocyanins, which are water-soluble flavonoid pigments synthesized in the cytoplasm, are stored in the vacuole through a microautophagy-like process (Sieńko *et al.*, 2020). Chanoca *et al.*, 2015a reported that anthocyanin aggregates in *Arabidopsis thaliana* and *Eustoma grandiorum* are directly incorporated into the vacuole through microautophagic mechanisms. This process involves the vacuolar membrane engulfing the aggregates without the participation of the ATG5 protein, PI3K complex, or SNARE components typically associated with macroautophagy. This finding highlights that certain ATG-independent pathways may exist in microautophagy. Here the microautophagyic machinery is different to the material to be degraded: While anthocyanin aggregates are processed by a pathway that does not relay on ATG5, chloroplasts and peroxisomes are degraded through microautophagy the depends on ATG5- and ATG7 (Chanoca *et al.*, 2015; Nakamura *et al.*, 2018; Oikawa *et al.*, 2022; Ding *et al.*, 2022).

Another critical aspect of microautophagy in plants is its role in chloroplast degradation, a process known as chlorophagy. Nakamura *et al.*, 2018 showed that exposure to high visible

light causes damage and swelling in chloroplasts within Arabidopsis mesophyll cells. Following this photodamage, the tonoplast invaginates the affected chloroplasts, allowing them to be transported into the vacuole through microautophagy. Sieńko *et al.*, 2020 reported that "GFP-ATG8-labelled structures were localized at the swollen chloroplasts after the damage, but they never covered the entire chloroplast". This selective process suggests that specific ATG proteins are necessary for the completion of chlorophagy, particularly the ATG8-containing membrane structure that resembles the micropexophagy process in yeast (Sieńko *et al.*, 2020). Other functions are similar to macroautophagy processes: During periods of nutrient scarcity, microautophagy allows plant cells to degrade and recycle intracellular components to maintain essential metabolic processes. This is particularly important for plants, which cannot relocate and must survive under fluctuating environmental conditions.

Microautophagy plays a role in the quality control of cellular organelles and proteins. By selectively degrading damaged or dysfunctional components, it prevents the accumulation of cellular debris that could impair cellular function or lead to oxidative stress (Sieńko *et al.*, 2020; Nakamura *et al.*, 2018).

Megaautophagy

Megaautophagy is a form of autophagy that involves the degradation of large cytoplasmic structures or organelles. Unlike micro- and macroautophagy, which typically target individual components, megaautophagy can accommodate larger cargo, such as entire organelles or protein aggregates. This process is particularly significant during programmed cell death (PCD), where the vacuole ruptures and releases hydrolases that degrade cellular constituents, ultimately leading to cell death (Van Doorn and Woltering, 2005). This terminal phase of megaautophagy marks an irreversible progression towards cell death, contributing significantly to tissue remodeling and development. Despite its importance, the molecular mechanisms and regulatory pathways of megaautophagy are less understood, and current knowledge is primarily based on morphological studies rather than molecular analyses (Yagyu and Yoshimoto, 2024).

Chaperone-Mediated Autophagy (CMA)

Chaperone-mediated autophagy (CMA) is a selective autophagy process specifically targeting proteins in the cytosol for degradation and depends on chaperone HSC70 and co-chaperones,

has been reported in mamalian cells but not in yeast and plants yet (Zhuang and Jiang, 2019; Mizushima and Komatsu, 2011). This process is unique as it does not involve the formation of autophagosomes. Instead, chaperone proteins recognize and bind to target proteins containing a specific pentapeptide motif (KFERQ-like sequence) and deliver them to the lysosomal membrane. The proteins are then translocated across the membrane into the lysosome for degradation (Orenstein and Cuervo, 2010).

However, selective autophagy processes similar to CMA are thought to exist in plants, particularly in the degradation of oxidized or damaged proteins, contributing to cellular quality control and stress responses (Michaeli *et al.*, 2016; Zhuang and Jiang, 2019).

Organelles-Specific Autophagy: Chlorophagy and Pexophagy

Selective autophagy is essential for maintaining cellular homeostasis by degrading specific organelles, including peroxisomes, mitochondria, and chloroplasts (Veljanovski and Batoko, 2014). This process can be either selective, targeting damaged or dysfunctional organelles, or non-selective, involving the general recycling of cellular components. Key proteins such as p62 and NBR1 serve as substrates and cargo receptors in animal cells by binding to ubiquitinylated proteins and containing an Atg8 interacting motif (Johansen and Lamark, 2011). In plants, AtNBR1 functions as a selective autophagy adaptor protein, combining features of animal NBR1 and p62 (Svenning *et al.*, 2011; Zientara-Rytter and Sirko, 2014; Romero-Barrios and Vert, 2018).

Research on the selective degradation of organelles—termed mitophagy, pexophagy, and chlorophagy—has revealed critical components involved in these processes. These mechanisms are vital for removing damaged organelles and maintaining cellular quality control, especially in plants where chlorophagy and pexophagy are crucial under stress conditions that may lead to organelle damage (Yoshitake *et al.*, 2021).

Chlorophagy

Chloroplasts, due to their role in photosynthesis, are constantly exposed to reactive oxygen species (ROS), which can damage their components. Chlorophagy helps remove these damaged chloroplasts, thereby preventing cellular damage and maintaining cellular homeostasis. Under stress conditions, such as high light intensity, nutrient deprivation, or pathogen attack, chlorophagy is upregulated to prevent the accumulation of damaged

chloroplasts, which could otherwise produce harmful ROS and lead to cellular damage. By removing these damaged organelles, chlorophagy helps to mitigate stress and protect the cell from oxidative damage. In addition to its role in stress response, chlorophagy is also involved in developmental processes, such as leaf senescence, deprivation and the transition from vegetative to reproductive growth. During these stages, the controlled degradation of chloroplasts allows for the recycling of nutrients and the reallocation of resources to support new growth or seed development (Nakamura and Izumi, 2018; Nakamura and Izumi, 2019; Kikuchi *et al.*, 2020).

Research has identified several autophagy-related (ATG) proteins involved in chlorophagy. For example, the ATG8 protein is crucial for the formation of autophagosomes and the recognition of damaged chloroplasts. Mutants which are deficient in ATG proteins, such as lack of ATG5 or ATG7, show defects in chlorophagy, leading to the accumulation of damaged chloroplasts and increased sensitivity to stress conditions (Nakamura and Izumi, 2019). The exact mechanism of chlorophagy is still not fully investigated, but some components and steps have been identified so far:

Pathways of chloroplast degradation can either be of macroautophagic or microautophagic nature. As mentioned before, microautophagy of chloroplasts involves the direct invagination of chloroplast contents into the vacuole membrane. High-intensity light (HL) can induce damage to the chloroplast envelope, leading to chloroplast swelling, as observed in studies by Nakamura *et al.*, 2018. Additionally swollen chloroplast were found in the vacuole under these conditions, when there is an overexpression of the VESICLE INDUCING PROTEIN IN PLASTID1 (VIPP1), which helps to maintain the chloroplast envelope integrity (Sieńko *et al.*, 2020). Chloroplasts are identified by structures that contain ATG8 prior to their engulfment by the tonoplast into the vacuole. In the atg5 mutant, this process does not take place, which implies that an ATG-dependent microautophagy-like mechanism may be involved (Nakamura and Izumi, 2019; Zhuang and Jiang, 2019).

The role of ATG8-labeled structures might be to selectively recognize chloroplasts through interactions with chlorophagy receptors, similar to how ATI-PS bodies are recognized. Alternatively, ATG8 may facilitate the fusion between the chloroplast membrane and tonoplast, releasing chloroplast contents into the vacuole. Other studies have described different structures involved in chloroplast degradation that resemble microautophagy, although they were not initially classified as such (Zhuang and Jiang, 2019).

Senescence-associated vacuoles (SAVs), for example, are a distinct type of lytic compartment found during leaf senescence, characterized by the presence of senescence-induced cysteine protease Senescence-associated gene 12 (SAG12) (Zhuang and Jiang, 2019). SAVs share characteristics with lytic vacuoles but lack the tonoplast marker γ-TIP. SAVs contain stromal proteins such as Rubisco and glutamine synthetase, but not thylakoid proteins (Izumi and Nakamura, 2018). Interestingly, SAVs are still formed in the atg7 mutant, indicating a separate pathway for chloroplast turnover (Zhuang and Jiang, 2019).

Under abiotic stresses chloroplast vesiculation (CV) leads to the accumulation of chloroplast-containing vesicles (CCVs), which are downregulated by cytokinin. These vesicles comprise various chloroplast components, including proteins from the stroma, envelope, and thylakoid, and they form independently of autophagy, as indicated by their absence of the autophagosome marker GFP-ATG8a (Wang and Blumwald, 2014). Research has shown that CV interacts with the PsbO protein of the photosystem II complex located on the thylakoid membrane, suggesting that CCVs may originate from within the chloroplast. Furthermore, recent findings indicate that the NAC transcription factor RD26, which is involved in ABA-related gene regulation, regulates CV. This implies a feedback loop between ABA signaling and the degradation of chloroplasts via CCVs (Kamranfar *et al.*, 2018; Zhang and Gan, 2012; Zhuang and Jiang, 2019). Nevertheless, the precise origins of SAVs and CCVs remain unclear, primarily due to the absence of observed intermediate structures (Zhuang and Jiang, 2019).

Macrochlorophagy pathways can be whole chloroplast degradation, or partly degradation of chloroplasts like the RCBs (RuBisCO containing bodies) pathway, ATI-PS pathway or SSTG (small starch granule-like) pathway.
The RCBs pathway requires ATG genes like ATG5 and ATG7 as well as ATG8. By forming these autophagic bodies the chloroplast is partly degraded. This pathway is induced under C-starvation and in starchless mutants. Moreover, RCBs appear to be closely related to extending stromules. These stromules are highly induced under different abiotic and biotic signals, like ROS or high sucrose content (Zhuang and Jiang, 2019). Unlike RCBs, ATI-PS were not detectable at stromules and differ in their cargo, as they carry thylakoid- and outer-envelope-proteins as well (Michaeli *et al.*, 2014). This process was supposed to be only distributed to the ER, but has recently also been observed on the outer chloroplast membrane upon sugar deprivation.

It is still debated, how ATI-PS are re-localized in the chloroplast lumen, as they are described to be single transmembrane protein of the ER. The ATI-PS degradation pathway is mediated by plant-exclusive ATI-proteins, which directly interact with ATG8 via the AIM motif. Interestingly, only the delivery to the vacuole is supposed to be ATG-depend (Michaeli *et al.*, 2014).

The SSTG (Small starch granule-like structure) pathway focuses on the export of starch from the chloroplast. Starch granules are distributed throughout the chloroplast and serve as a vital energy source by being converted into sugar when photosynthesis is unavailable, such as during the night. In *Arabidopsis thaliana*, transitory starch is synthesized during the day and subsequently degraded at night to fulfill the sugar demands of the cell. However, the exact mechanism of how starch granules are exported from the chloroplast remains largely unknown (Malinova *et al.*, 2018; Wang *et al.*, 2013; Liu *et al.*, 2013).

Wang et al. (2013) observed SSTGs being exported through stromules and proposed that leaf starch degradation may be mediated by a combination of autophagy and chloroplast pathways. Specifically, ATG6 has been identified as a key player in autophagy, as atg6-silenced *Nicotiana benthamiana* plants accumulate significantly higher levels of starch in their chloroplasts compared to other ATG mutants. In parallel, the *sex1* mutant, which is defective in starch degradation, exhibits elevated starch accumulation, suggesting that SEX1 plays a crucial role in leaf starch breakdown via the chloroplast pathway.

In addition, Wang et al. (2015) demonstrated that TUB8-silenced *N. benthamiana* and *A. thaliana* plants showed similar starch excess phenotypes, implicating the involvement of microtubules in starch degradation. Tubulins, as part of the microtubule network, have been shown to participate in stromule formation alongside actin filaments, suggesting that stromules may play a pivotal role in the SSTG pathway by facilitating the transport of SSTGs. While stromules in *N. benthamiana* are more dynamic and prominently associated with microtubules, stromules in Arabidopsis are less extensive but may still rely on microtubules for their formation and function.

An important, yet unresolved question regarding chlorophagy and other organelle-specific autophagy pathways is the role of receptor-specific membrane proteins, which may signal the cytoplasmic degradation machinery or act as docking stations for the autophagy or vacuolar processes. In macroautophagy, these proteins typically contain a canonical AIM (ATG8-interacting motif) and possess domains for cargo interaction, often through mechanism which are dependent or independent of ubiquitin (Zaffagnini and Martens, 2016). Albeit, in the

context of chlorophagy, key anchor proteins that connect the chloroplast to the microtubule network, especially those localized to the outer chloroplast membrane, remain unidentified (Zhuang and Jiang, 2019).

Microtubules

Microtubules are crucial components of the cytoskeleton in eukaryotic cells, providing structural support, enabling intracellular transport, and playing a vital role in cell division. These dynamic, cylindrical polymers are composed of α-tubulin and β-tubulin proteins that assemble into a hollow tube with a diameter of approximately 25 nm (Akhmanova and Steinmetz, 2008). The organization of tubulin dimers within microtubules creates a polar structure with distinct plus (+) and minus (-) ends. This polarity is essential for the dynamic behavior of microtubules and their involvement in various cellular processes (Zaffagnini and Martens, 2016). The formation of microtubules, or microtubule nucleation, occurs at microtubule-organizing centers (MTOCs) similar to centrosomes in animal cells or spindle pole bodies in plant cells (Haruta *et al.*, 2023). During nucleation, tubulin dimers polymerize, primarily at the plus end of the microtubule, leading to rapid growth and shrinkage in a process known as dynamic instability. This dynamic nature allows microtubules to rapidly reorganize in response to cellular needs, and it is tightly regulated by various microtubule-associated proteins (MAPs) that can stabilize or destabilize the microtubule structure (Zheng *et al.*, 1995). Microtubules are involved in several essential cellular functions such as cell division, cell shape and polarity and intracellular transport (Siegrist and Doe, 2007 Hirokawa *et al.*, 2009, McIntosh *et al.*, 2010).

As mentioned before, microtubules are strongly involved in the extension of stromules in *N. benthamina*, as stromules have been observed to move along microtubules, whereas actin filaments serve as anchoring points (Kumar *et al.*, 2018), thus organizing the movement of, e.g. chloroplasts. However, research is lacking in observation of the involvement of microtubules in stromule formation in *A. thaliana*.

The role of microtubules in autophagy has been extensively studied in various eukaryotic systems, including plants. Here microtubules are essential for the proper formation autophagosomes and they facilitate the movement of autophagosomes toward lysosomes, where these components are degraded. Disruption of microtubule dynamics can impair the transport of autophagosomes, thereby inhibiting the autophagic process (Köchl *et al.*, 2006).

Wang *et al.*, 2015 demonstrated that disrupting microtubule dynamics using pharmacological agents led to a significant reduction in autophagic flux, indicating that microtubules are required for efficient autophagosome movement towards the vacuole. This finding underscores the importance of the cytoskeletal network in maintaining the efficiency of autophagy, particularly under stress conditions that activate this degradation pathway. In addition to facilitating the movement of autophagosomes, microtubules also play a role in the spatial organization of the autophagic machinery within the cell. Wang *et al.*, 2016 found that certain microtubule-associated proteins (MAPs) directly interact with autophagy-related (ATG) proteins, suggesting that microtubules not only provide structural support but also participate in the regulatory mechanisms that coordinate autophagy. This interaction likely ensures that autophagosomes are efficiently formed and directed towards their final destination for degradation, thereby preventing the accumulation of damaged or unnecessary cellular components. Identifying these anchor proteins could significantly advance our understanding of stromule formation, their role in starch degradation, and the broader mechanisms governing plastid dynamics in *Arabidopsis*.

Identifiction of OEF18

In 2011, Dr. Roman Bayer and Dr. Simon Stael identified a calcium-binding protein named OEF18, located in the outer chloroplast envelope, weighing 18 kDa. Analysis showed OEF18 has two transmembrane domains and an EF-hand motif. In Arabidopsis, they found a similar protein, OEF18-like (OEF18L), which cannot bind calcium due to the replacement of negatively charged amino acids with positively charged lysine residues in the EF-hand motif (figure1)

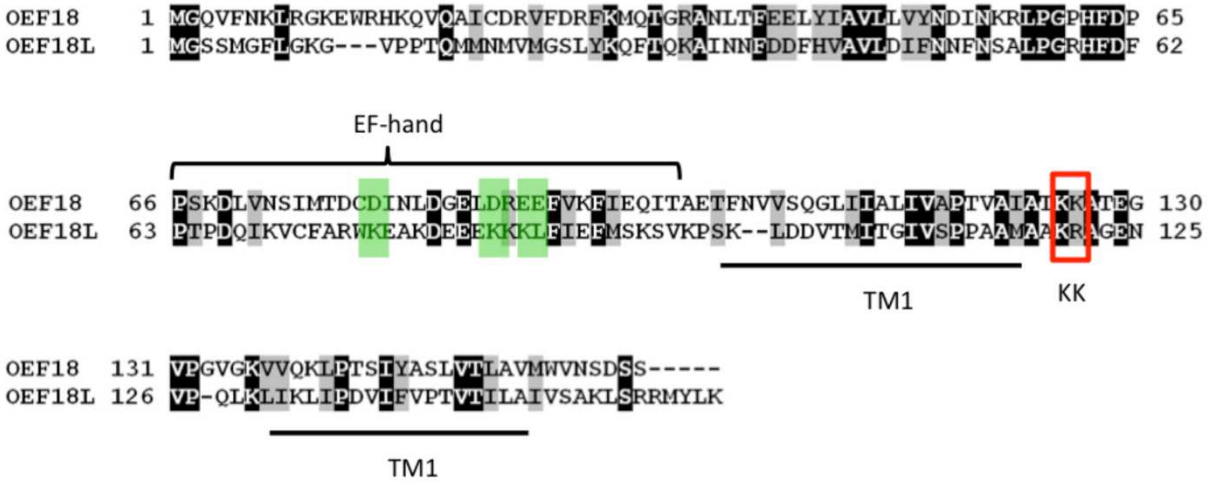

Figure 2: Sequence alignment of OEF18 and OEF18L. TM1 and TM2 – both trans-membrane domains; KK – double lysine motif. Provided by Dr. Przemyslaw Kmiecik.

Dr. Simon Stael discovered that plants lacking OEF18 have smaller leaves under long-day conditions, while plants overexpressing OEF18 have larger leaves. OEF18 is expressed in all leaf tissues except seeds, with high levels in cotyledons and aging leaves, and its expression increases under salt and osmotic stress (Kmiecik, 2018).

Przemyslaw Kmiecik's 2018 dissertation detailed OEF18's biochemical functions, confirming its presence in chloroplasts and peroxisomes, with both termini extending into the cytosol. Experiments confirmed OEF18's calcium-binding ability, showing that the N-terminal EF-hand motif is responsible, while a mutant (D79A) failed to bind calcium. The CD spectra indicated proper folding of the EF-hand motif and structural integrity post-mutation (Kelly *et al.*, 2005) an size exclusion experiments indicated, that OEF18 forms tetramers upon calcium binding.

OEF18 has been suggested to interact with tubulins, which has been observed in co-immunoprecipitation (co-IP) experiment and unbiased Yeast-two-hybrid (Y2H) screen, suggesting a role in communication or movement between organelles, as both peroxisomes and chloroplasts depend on the cytoskeleton for positioning. Western blots indicated that OEF18 might facilitate calcium-dependent interactions between peroxisomes and chloroplasts, with wild-type chloroplasts showing increased peroxisomal association in the presence of calcium, a response not seen in oef18 mutants. However, the overexpression of OEF18-Strep and results from oef18/oef18l double mutants complicated the interpretation, possibly indicating artificial interactions due to overexpression (Kmiecik, 2018).

Ubiquitin was identified as an interaction partner in the mY2H assay, suggesting a role in chloroplast stress response. Although OEF18 is not predicted to be directly ubiquitinated (UbPred, http://www.ubpred.org/; (Radivojac *et al.*, 2010)), its interaction with ubiquitin suggests an indirect role in related processes. OEF18L contains a predicted ubiquitination site, but both OEF18 and OEF18L lack typical ubiquitin-interacting motifs (ScanProsite, https://prosite.expasy.org/scanprosite/; de Castro *et al.*, 2006). The interaction with ubiquitin warrants further investigation, as oxidative stress-induced chloroplast damage leads to ubiquitin-mediated degradation via E3 ubiquitin ligases like PUB4 and SP1 (Woodson *et al.*, 2015; Ling and Jarvis, 2015; Ling and Jarvis, 2016), but this will not be termed in this master's thesis.

OEF18's high accumulation in aging leaves supports its involvement in senescence, potentially through autophagy. The dual localization of OEF18 supports this hypothesis, as both

peroxisomes and chloroplasts are actively degraded during natural and stress-induced senescence (Avin-Wittenberg, 2018). The reduced formation of BTH-dependent vesicles in oef18 knockout lines indicates a potential role for OEF18 in autophagy. OEF18 has an Atg8-interacting motif (AIM) and may function in selective autophagy, acting as an adapter between autophagy-related vesicles and the ATG8-dependent autophagy machinery. In follow-up experiments done by Dr. Bernhard Wurzinger and Dr. Przemyslaw Kmiecik interactions with ATG8 could not be observed, excluding an actual function of the AIM-site and a direct interaction with ATG8. To determine whether OEF18 is involved in chloroplast degradation, growth experiments will be carried out under different abiotic stress conditions like heat stress and highlight stress and starvation conditions, to induce autophagy.

OEF18's potential interaction with tubulin beta chains is intriguing from an autophagy perspective, as they were observed in a co-IP experiment and an unbiased membrane Y2H screen (Kmiecik, 2018). In mammalian cells, autophagosome formation, maturation, and fusion with lysosomes depend on an intact microtubule cytoskeleton (Mackeh *et al.*, 2013). In Arabidopsis, ATG8 and ATG4 proteins interact with tubulin, and ATG8 co-localizes with the microtubule cytoskeleton (Ketelaar *et al.*, 2004). The tobacco NBR1-like protein JOKA2, a cargo receptor, co-localizes with microtubules and microfilaments both alone and as part of the ATG8-JOKA2 complex (Zientara-Rytter and Sirko, 2014). Additionally, ATG6 interacts with tubulin beta chains, and disruption of the microtubule cytoskeleton reduces autophagosome formation under stress (Wang *et al.*, 2015), correlating with a starch-excess phenotype and underscoring the necessity of autophagy for leaf starch degradation. Wang *et al.*, 2015 revealed that β-Tubulin8 is involved in starch excess (SEX) chlorophagy, which is proposed to be a potential interaction partner of OEF18. A MT assay was already performed by Dr. Przemyslaw Kmiecik using the MT Binding Protein Spin-down kit from Cytoskeleton, Inc. (Cat. #BK029), but OEF18 could not be detected. This suggests, assuming an interaction of OEF18 and tubules, that OEF18 may only act as an anchor protein, interacting at very few points of tubules. According to this, in this thesis, experiments proving the interaction of OEF18 with β-tubulins by a biased Y2H assay are assed.

Lugol's staining and an enzymatic quantitative starch degradation assay of plant leaves of different plant lines, done by Dr. Przemyslaw Kmiecik, revealed that the *oef18* single knockout and *oef18/oef18l* double knockout lines accumulate starch at the end of the night, unlike the wildtype (and the other plant lines), which degrades (almost) all transitory starch during the

night (fig. 2), merging to the results of silenced β-Tubulin8 in Wang *et al.*, 2015. Due to a possibly lower starch degradation efficiency of OEF18-lacking plants the starch accumulation at the end of the day is higher as well. This would also include an involvement of OEF18 in the SEX chlorophagy process. To solidify this assumption the experiment will be repeated in this master's thesis.

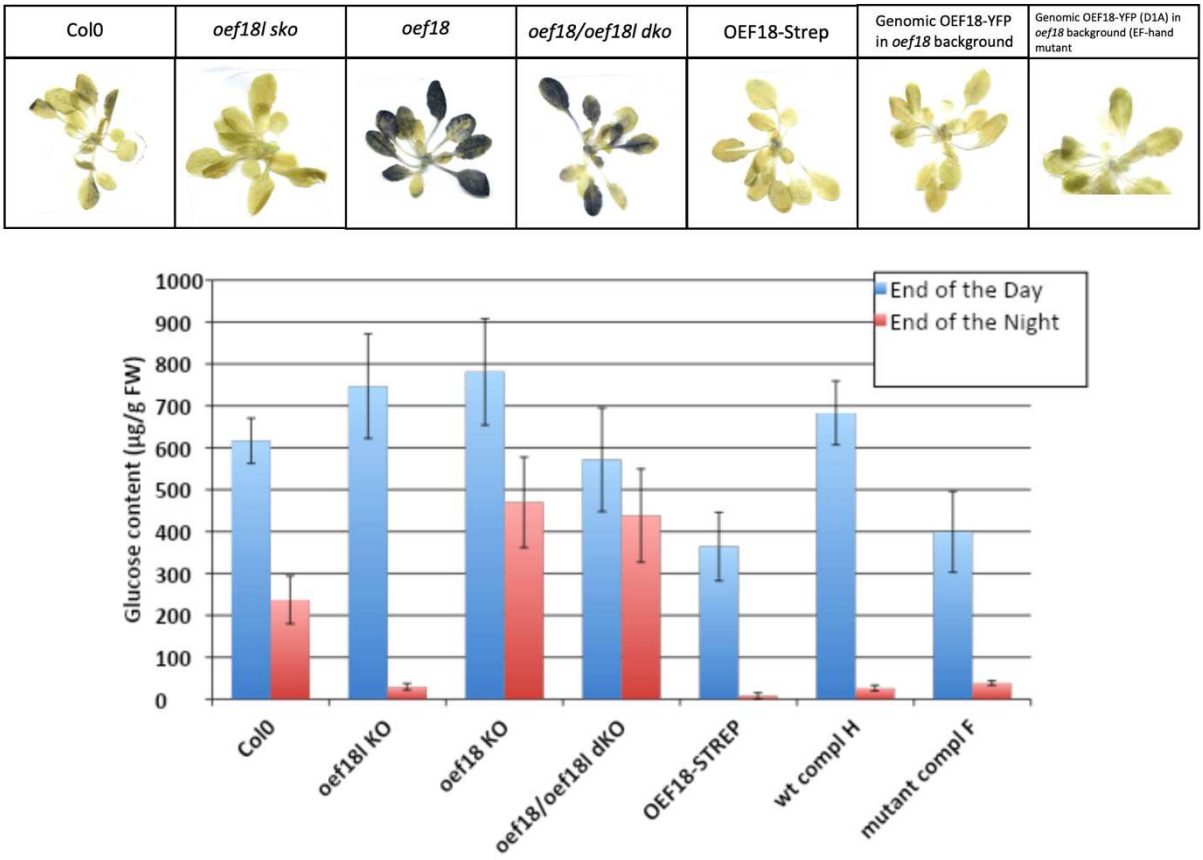

Figure 2: Comparative starch detection of 4-week-old Arabidopsis plants grown under normal grown conditions in 16/8 light dark rhythm. A) Lugols staining of Arabidopsis leaves. B) Enzymatic quantitative starch detection. The experiments have been carried out by Dr. Przemylaw Kmiecik.

Moreover, in this Master's thesis the impact of OEF18 on stromule formation will be observed. In the dissertation of Prezmylaw Kmiecik OEF18-YFP was observed in these stromules protruding from chloroplasts. Since it is assumed that OEF18 interacts with tubules and tubules are thought to be involved in stromule formation, the *oef18/oef18l* double knockout lines and OEF18-Strep overexpression lines will be tested on differences in the stromule formation.

Taken together the questions addressed in this master's thesis are:

1. Investigate the role of OEF18 in the stromule formation in chloroplasts

2. Examine OEF18s involvement in chlorophagy under stress conditions
3. Determine if OEF18 interacts with β-tubulin, potentially influencing microtubule-related processes like autophagosome-formation or stromule-extension

2 Material and Methods

2.1 Material

2.1.1 Vectors

3171 pBIB aleurin-pHsensor sCherry	Binary vector-backbone used for transformation of Arabidopsis thaliana and transient expression in tobacco leaves (nicotiana tabacum), provided by Dr. Jose Julián Valenzuela
RBCS_YFP_sCherry	Binary vector used for transformation of Arabidopsis thaliana and transient expression in Tobacco leaves (nicotiana tabacum); protein of interest (Ribulose-1,5-bisphosphat-carboxylase-oxygenase (RuBisCO) small subunit) is fused with yellow fluorescent protein (YFP) enabling the in-vivo localization analysis of stroma. Contains Kanamycin resistance and seed code marker sCherry. Successfully transformed Arabidopsis seeds will express red fluorescent seed code marker.
CFP_[SKL]_sCherry	Binary vector used for transformation of Arabidopsis thaliana and transient expression in tobacco leaves (nicotiana tabacum); cyan fluorescent protein (CFP) is fused with peroxisome targeting sequence [SKL] enabling the in-vivo localization analysis of peroxisomes. Contains. Kanamycin resistance and seed-code-marker sCherry. Successfully transformed Arabidopsis seeds will express red fluorescent seed code marker.
pGBKT7	Binary vector used for yeast two hybrid assay. Protein of interest was N-terminally fused to GAL4 DNA binding domain. Contains TRP1 gene and Neomycin- and Kanamycin resistance genes.
pGAD424	Binary vector used for yeast two hybrid assay. Protein of interes was N-terminally fused to GAL4 activating domain. Contains LEU2 gene and Ampicilin resistance gene.

2.1.2 Primers

RuBisCO SSU forward	gagtttttctgattaacagaATGGCTTCCTCTATGCTCTC
RuBisCO SSU reverse	tagaaaccatACCGGTGAAGCTTGGTGG
YPET forward	cttcaccggtATGGTTTCTAAAGGTGAAG
YPET revers	gaaattcgagctcggtacccTCATTTGTACAATTCATTCATAC

Mturquoise forward	gagtttttctgattaacagaATGGTTTCTAAAGGTGAAG
Mturquoise reverse	ttgcctccatTTTGTACAATTCATCCATACC
CFP-[SKL] forward	gagtttttctgattaacagaATGGTTTCTAAAGGTGAAG
CFP-[SKL] reverse	gaaattcgagctcggtacccTCAAAGCTTAGATTTGTACAATTC
pGAD424 β-tubulin 1 forward	aaaaaagagatcgaattccccATGAGAGAAATCCTCCAC
pGAD424 β-tubulin 1 reverse	ctgcaggtcgacggatccccTCAAGATTCGTAAACTTGTTC
pGAD424 β-tubulin 2 forward	aaaaaagagatcgaattccccATGCGTGAGATTCTTCAC
pGAD424 β-tubulin 2 reverse	ctgcaggtcgacggatccccTCAGTACTCTTCCTCCTG
pGAD424 β-tubulin 3 forward	aaaaaagagatcgaattccccATGCGTGAGATTCTTCAC
pGAD424 β-tubulin 3 reverse	ctgcaggtcgacggatccccTCAGTACTCTTCTTCCTG
pGAD424 β-tubulin 4 forward	aaaaaagagatcgaattccccATGAGAGAGATCCTTCATATC
pGAD424 β-tubulin 4 reverse	ctgcaggtcgacggatccccTTAAGTCTCGTACTCCTC
pGAD424 β-tubulin 5 forward	aaaaaagagatcgaattccccATGAGAGAGATCCTTCAC
pGAD424 β-tubulin 5 reverse	ctgcaggtcgacggatccccTCAAGTCTCATAATCTCCC
pGAD424 β-tubulin 6 forward	aaaaaagagatcgaattccccATGAGAGAAATCCTTCACATTC
pGAD424 β-tubulin 6 reverse	ctgcaggtcgacggatccccTCACTCATGATCCAATATCTC
pGAD424 β-tubulin 7 forward	aaaaaagagatcgaattccccATGCGTGAGATTCTTCATATTC
pGAD424 β-tubulin 7 reverse	ctgcaggtcgacggatccccTCAATAAGTTTCTTCTTGCTC
pGAD424 β-tubulin 8 forward	aaaaaagagatcgaattccccATGCGAGAGATTCTTCAC
pGAD424 β-tubulin 8 reverse	ctgcaggtcgacggatccccTTATTGCTCCTCCTGCAC
pGAD424 β-tubulin 9 forward	aaaaaagagatcgaattccccATGAGAGAAATTCTTCATATTCAAG
pGAD424 β-tubulin 9 reverse	ctgcaggtcgacggatccccTTAGGCTTCTTCTTCTTCTTC
pGAD424 OEF18 forward	aaaaaagagatcgaattccccATGGGACAAGTCTTTAAC
pGAD424 OWF18 reverse	ctgcaggtcgacggatccccTTAACTTGAATCAGAATTCACC
pGAD424 OEF18-like forward	aaaaaagagatcgaattccccATGGGTAGTTCAATGGGC
pGAD424 OEF18-like reverse	ctgcaggtcgacggatccccCTATTTCAAATACATTCGTCTAGAG

pGBKt7 β-tubulin 1 forward	gccatggaggccgaattccccATGAGAGAAATCCTCCAC
pGBKt7 β-tubulin 1 reverse	ctgcaggtcgacggatccccTCAAGATTCGTAAACTTGTTC
pGBKt7 β-tubulin 2 forward	gccatggaggccgaattccccATGCGTGAGATTCTTCAC
pGBKt7 β-tubulin 2 reverse	ctgcaggtcgacggatccccTCAGTACTCTTCCTCCTG
pGBKt7 β-tubulin 3 forward	gccatggaggccgaattccccATGCGTGAGATTCTTCAC
pGBKt7 β-tubulin 3 reverse	ctgcaggtcgacggatccccTCAGTACTCTTCTTCCTG
pGBKt7 β-tubulin 4 forward	gccatggaggccgaattccccATGAGAGAGATCCTTCATATC
pGBKt7 β-tubulin 4 reverse	ctgcaggtcgacggatccccTTAAGTCTCGTACTCCTC
pGBKt7 β-tubulin 5 forward	gccatggaggccgaattccccATGAGAGAGATCCTTCAC
pGBKt7 β-tubulin 5 reverse	ctgcaggtcgacggatccccTCAAGTCTCATAATCTCCC
pGBKt7 β-tubulin 6 forward	gccatggaggccgaattccccATGAGAGAAATCCTTCACATTC
pGBKt7 β-tubulin 6 reverse	ctgcaggtcgacggatccccTCACTCATGATCCAATATCTC
pGBKt7 β-tubulin 7 forward	gccatggaggccgaattccccATGCGTGAGATTCTTCATATTC
pGBKt7 β-tubulin 7 reverse	ctgcaggtcgacggatccccTCAATAAGTTTCTTCTTGCTC
pGBKt7 β-tubulin 8 forward	gccatggaggccgaattccccATGCGAGAGATTCTTCAC
pGBKt7 β-tubulin 8 reverse	ctgcaggtcgacggatccccTTATTGCTCCTCCTGCAC
pGBKt7 β-tubulin 9 forward	gccatggaggccgaattccccATGAGAGAAATTCTTCATATTCAAG
pGBKt7 β-tubulin 9 reverse	ctgcaggtcgacggatccccTTAGGCTTCTTCTTCTTCTTC
pGBKt7 OEF18 forward	gccatggaggccgaattccccATGGGACAAGTCTTTAAC
pGBKt7 OEF18 reverse	ctgcaggtcgacggatccccTTAACTTGAATCAGAATTCACC
pGBKt7 OEF18-like forward	gccatggaggccgaattccccATGGGTAGTTCAATGGGC
pGBKt7 OEF18-like reverse	ctgcaggtcgacggatccccCTATTTCAAATACATTCGTCTAGAG

2.1.3 Bacteria strains

DH5alpha	E. coli strain used for cloning. Genotype: huA2 Δ(argFlacZ)U169 phoA glnV44 Φ80 Δ(lacZ)M15 gyrA96 recA1 relA1 endA1 thi---1 hsdR17
Agl1	*recA::bla* pTiBo542ΔT Mop+ CbR

2.1.4 Yeast strains

PJ69-4alpha	Yeast strain used for yeast two hybrid assay

2.1.5 Plant lines

Col0	Arabidopsis thaliana wild type with Colombia ecotype
OEF18-Strep	Stable Arabidopsis Col0 line overexpressing full length OEF18 C-terminally fused with Strep tag under control of 35S promotor; BASTA resistance marker; provided by Dr. Przemylaw Kmiecik
oef18-1	T-DNA insertion line for OEF18 in Col0 background; BASTA resistance marker (WiscDsLox461-464A5); provided by Dr. Przemylaw Kmiecik
oef18-2	T-DNA insertion line for OEF18 in Col4 background; BASTA resistance marker (SK40148); provided by Dr. Przemylaw Kmiecik
oef18L	T-DNA insertion line for OEF18L in Col0 background; Kanamycin resistance marker (SALK_022186.56.00.x); provided by Dr. Przemylaw Kmiecik
oef18/oef18l	double T-DNA insertion line for OEF18 and OEF18L generated by crossing the oef18l line into oef18-1 background; BASTA and Kanamycin resistance marker; provided by Dr. Przemylaw Kmiecik
oef18 EF-hand mutant	genomic OEF17 D1A-YFP in oef18-1 background; inactive EF-hand; provided by Dr. Przemylaw Kmiecik
atg5	T-DNA insertion from NASC collection; BASTA resistance marker; provided by Marintia Nava
Nicotiana tabacum cv.	

Petite Havana SR1

2.1.6 Media

Lysogeny broth (LB)	For the liquid media 10 g tryptone, 10 g NaCl, 5 g yeast extract were dissolved and pH was adjusted to 7.2 with NaOH. For plates additionally 20 % of agar was added before autoclaving. For selective media following concentrations of antibiotics were used: ampicillin – 100 µg/ml, kanamycin – 50 µg/ml, gentamycin – 10 µg/ml, and rifampicin – 25 µg/ml.
Yeast extract beef medium (YEB)	For the liquid media 10 g/l peptone and 1 g/l yeast extract were dissolved in 5 % w/v sucrose and 0.5 g/l $MgCl_2$ were dissolved in water.
½ Murashige-Skoog medium (1⁄2 MS)	For the liquid media 2.2 g Murashige-Skoog powder (Duchefa) was dissolved and the pH was adjusted to 5.8 with 200 mM KOH.
½ MS plates for plant	½ MS, 1 % w/v Sucrose and 0.8 % plant Agar (Duchefa) was dissolved in water and the pH was adjusted to 5.8 with 200 mM KOH, before the media was autoclaved. For selective media following concentrations of antibiotics were used: ampicillin – 100 µg/ml, kanamycin – 50 µg/ml, gentamycin – 10 µg/ml, and rifampicin – 25 µg/ml.
Control media (Growth assay)	½ MS (Duchefa), 0.5 % MES w/v and 1 % w/v Sucrose were dissolved in water and the pH was adjusted to 5.8 with 200 mM KOH, before the media was autoclaved.
Carbon-starvation media (Growth assay)	½ MS (Duchefa)and 0.5 % MES w/v were dissolved in water and the pH was adjusted to 5.8 with 200 mM KOH, before the media was autoclaved.
Nitrogen-starvation media (Growth assay)	nitrogen-deficient ½ MS (0.39 g/l) (PhytoTech), 0.5 % MES w/v and 1 % w/v Sucrose were dissolved in water and the pH was adjusted to 5.8 with 200 mM KOH, before the media was autoclaved.

Bortezomib-treatment media (Growth assay)	½ MS (Duchefa), 0.5 % MES w/v and 1 % w/v Sucrose were dissolved in water and the pH was adjusted to 5,8 with 200 mM KOH, before the media was autoclaved. After that 3.75 µM Bortezomib were added.
TAE	40 mM Tris acetate; 1mM EDTA
YNB	4.6 g/l YNB (Yeast nitrogen base), 2 % glucose, 10 ml sterile filtered 100x amino acid stock
100x amino acid stock (-Leu, -Trp, -His, - Ade)	Sterile filtered; 3 g/l arginine, 2 g/l isoleucine, 4 g/l lysin, 2 g/l methionine, 6 g/l phenylalanine, 15 g/l threonine, 4 g/l tyrosine, 4 g/l uracil, 6.5 g/l valine, 10 g/l aspartate
100x Histidine stock	Sterile filtered; 2 g/l histidine
100x Adenine stock	Sterile filtered; 4 g/l adenine
50% PEG (3350)	50 % v/v PEG (3350)
LiAc	2 M lithium acetate

2.2 Methods

2.2.1 DNA

2.2.1.1 Cloning

The sequences of the genes were obtained from TAIR (www.arabidopsis.org). The primers were designed via NEBuilder assembly tool (www.nebuilder.neb.com) in the way that overhangs of the inserts were produced to ensure the ligation with using Nebuilder HiFi DNA Assembly Master Mix (New England Biolabs) according to manufactory's protocol. The backbone of the plasmid was provided by Jose: pBIB aleurain-pHsensor-sCherry, containing a Kanamycin resistance gene and a red fluorescent seed code marker (sCherry), as well as a UBQ10 promotor and a NOS terminator sequence. The aleurain-pHsensor-part, having a HindIII restriction site at the 5'-end and a SmaI site at the 3'-end, was cut out through

restriction digest according to NEB Restriction Enzyme Double Digestion protocol. The remaining vector was used as a backbone for the following inserts. The PCR products were the ligated into the vector using NEBuilder HiFi DNA Assembly Master Mix (NEB) according to manufactures protocol and sequenced (Microsynth; whole plasmid sequencing). Supplementory table 1 contains the primers used in this work.

2.2.1.2 Polymearese chain reaction (PCR)

For the cloning purposes the Q5 High-fidelity DNA Polymerase (NEB) was used according to the manufacturer's protocol. The PCR reaction was performed in three steps: 3 minutes at 95 °C followed by usually 35 cycles of 20 seconds at 95 °C, 30 seconds at 58 °C (sometimes the annealing temperature was adjusted according to the primer) and 1 minute per 1000 bp of the product at 72 °C. After the 35 cycles the reaction was followed by a 10 minute step at 72 °C. The products of the PCR reaction were then separated on agarose gel (0.7-1.6 %) and visualized using Midori Green Advanced DNA stain. For cloning purposes the appropriate band was excised from gel and DNA was purified using GeneJet Gel Extraction kit (thermo Scientific) according to manufacturer's protocol.

2.2.1.3 Agarose gel electrophoresis

Agarose gel electrophoresis was used for the separation and purification of PCR products, and analysis of plasmid control digests. The nucleic acid sample was mixed with the 10x loading buffer (50% glycerol, 0.05 % w/v bromphenol blue, 0.05 % w/v xylencyanol filled up in 1x TAE buffer (40 mM Tris pH 8.0, 20 mM acetic acid, 1 mM EDTA)) and separated on the 0.7-1.6 % agarose gel (depending on the separation characteristic required) prepared with 1xTAE buffer supplemented with 3 µl per 50 ml 1x TAE buffer Midori Green Advanced DNA stain (NIPPON Genetics European GmbH). The UV light was used to visualize the nucleic acids stained with cyber green in ChemiDoc™ XRS+ Software (Bio-Rad).

2.2.2 Bacteria

2.2.2.1 Heat shock transformation E.coli

The ligation of DNA fragments was performed using Nebuilder HiFi DNA Assembly Master Mix (NEB) according to manufactory's protocol. After that 2 µl of ligation reaction (40-80 ng DNA) was mixed with 100 µl of competent E. coli strain and the suspension was incubated on ice for

30 min. The heat shock was performed by incubation of the tube at 42 °C for 1 min, followed by resting on ice for 2 min. After that 700 µl of LB-medium was added to the suspension and then incubated at 37 °C for 1 h for recovery. After that the suspension was centrifuged at 12000 g for 1 min at room temperature. The supernatant was discarded and 150 µl fresh LB-medium were added to the pellet and re-suspended, before it was spread on appropriate selection plates.

2.2.2.2 Heat shock transformation A.tumefaciens

The ligation of DNA fragments was performed using Nebuilder HiFi DNA Assembly Master Mix (NEB) according to manufactory's protocol. After that 100 ng/µl of ligation reaction was mixed with 50 µl of thermo-competent A.tumefaciens strain and the suspension was incubated on ice for 30 minutes. The heat shock was performed by a previous incubation in liquid nitrogen for 1 min before incubating the tube at 30 °C for two minutes. After that 700 µl of YEB-medium was added to the suspension and the incubated at 30 °C for 2 h for recovery. After that the suspension was centrifuged at 12000 g for 1 min at room temperature. The supernatant was discarded and 150 µl fresh YEB-medium were added to the pellet and re-suspended, before it was spread on appropriate selection plates.

2.2.2.3 MiniPrep

E.coli strain was scratched out on appropriate selective LB-Plate and incubated over night at 37 °C. One colony was inoculated in 5 ml selective LB-medium and again incubated over night at 37°C 200 rpm. After that the culture was centrifuged (2x 2 ml in 2 ml Eppendorf tube) at 12000 g for 1 min at room temperature, and the supernatant discarded. 300 µl P1 buffer (50 mM Tris pH 8, 10 mM EDTA and 100 mg/l RNase A) were added and the pellet fully re-suspended. After that 300 µl P2 buffer (200 mM NaOH, 1 % SDS) were added and the Eppendorf tubes carefully inverted. Then 300 µl P3 buffer (3 M KAc pH 5.5) were added and the tubes inverted. The suspension was centrifuged for 10 min at 4°C at 12000 g for 10 min. The supernatant (~850 µl) was transferred into a new 2 ml Eppendorf tube and 850 µl 2-propanol were added the tubes inverted and then centrifuged for 30 minutes at 12000 g at 4 °C. The supernatant was discarded and the Pellet re-suspended in 200 µl ice-cold 70 % ethanol and again centrifuged at 4 °C, 12000 g for 5 min. The supernatant was discarded and the tubes were dried for 30 minutes before they were re-suspended in 35 µl H_2O.

2.2.3 Yeast

2.2.3.1 Yeast transformation (Quick and dirty)

Transformation-mix (3200 µl sterile filtrated 50 % PEG (3300), 400 µl sterile filtrated 2 M LiAc, 400 µl 1M Dithiothreitol, 40 µl ssDNA and freshly scratched PJ69-4alpha yeast cells) was given to 2 µg of DNA (per plasmid) and was incubated for 20 min at 30 °C and after that for 20 min at 42 °C, both without shaking. Then 1 ml of H_2O was added to each reaction tube, mixed thoroughly and the suspension was centrifuged for 1 min at 4000 rpm and the cell pellet diluted in 100 µl sterile H_2O. The suspension was then plated on SD-Leu-Trp plates and incubated for 2-3 days at 30 °C.

2.2.3.2 Yeast-two-hybrid assay

First a dilution series of the different yeast colonies was prepared. 2 ml overnight culture were inoculated in appropriate SD-medium and diluted to an OD_{600} of 0.25 and after that grown until an OD_{600} of 1.0. From those cultures a 1:10, 1:100 and 1:1000 dilution has been prepared, and plated out on -Leu-Trp, -Ade-Leu-Trp and -His-Ade-Leu-Trp SD-plates.

2.2.4 Plants

2.2.4.1 Seed sterilization

Seeds were sterilized under the fume hood with chlorine gas. For this the seeds were placed in open *Eppendorf* tubes in a desiccator. In a beaker 100 ml 37 % HCl was added up with 150 ml HOCl from Danclorix, and incubated for 2 h. The Eppendorf tubes were rested for another 30 minutes under the fume hood to get of the chlorine gas.

2.2.4.2 Growth assay in liquid media

In a 6-well plate 2.5ml of growth media (control media) was added in every well. In every well around 50 seeds were added and stratified for 3 days at 4 °C in darkness. After that the seeds were grown for 9 days at 22 °C 16 h/8 h cycle (150 µE light intensity) at 90 rpm. After 9 days the starvation assays started. The control media was replaced with the new corresponding media, after rinsing it twice with it (Carbon starvation media for carbon starvation, Nitrogen starvation media for nitrogen starvation). The control well-plates were rinsed twice with control media, the bortezomib-treatment plates were rinsed twice with bortezomib (3.75 µM) containing media. For the carbon starvation growth assay, the carbon starvation seeds and the control seeds were kept for 4 days in darkness at 22 °C at 90 rpm. The Nitrogen Starvation and

the bortezomib-treatment growth assays stayed at the same light conditions as in growth state (6 days for N-Starvation and 9 days for bortezomib-treatment).

2.2.4.3 Growth assay

Growth assay agar plates

Sterilized seeds were sawn on agar plates (0,8% plant agar, ½ MS-media, 1% Sucrose, pH 5,8) and stratified for 3 days. After that they were transferred to growing chambers for 3 days under long day growth conditions (150 µE, 22°C). Then the 3-day-old seedlings were transferred to a control plate and a nitrogen-starvation plate and grown for 6 days under long day conditions. The Bortezomib plate was prepared according to the liquid media, with the addition of 0.8 % plant agar.

Growth assay in soil

Sterilized seeds were sawn on agar plates (0,8% plant agar, ½ MS-media, 1% Sucrose, pH 5,8) and stratified for 3 days. After that they were transferred to growing chambers for 7 days under long day growth conditions (150 µE, 22°C). After 7 days the seedlings were transferred into soil (3 per pot) and after 3 days the best-looking plant is left, whereas the other two seedlings are discarded. The remaining seedling will grow for 14 days in total in soil. After that the stress conditions will start.

Highlight stress:

The 3-week-old plant is transferred into a growing chamber with highlight conditions: 680 µE, 22 °C, long day conditions (16h/8h). The Highlight stress will last for 3 days. After that the photosynthetic parameters using the Imaging PAM Mini (WALZ) were measured.

Heat stress:

The 3-week-old plant is transferred into a growing chamber with heat stress conditions: 150 µE, 37 °C, long day conditions (16h/8h). The Highlight stress lasted for 3 days. After that the is transferred back to normal growing conditions for recovery for 7 days. After that the photosynthetic parameters using the Imaging PAM (WALZ) Mini were measured.

2.2.4.4 Transient expression in tobacco leaves

The overnight cultures for Agrobacteria GV3101 stocks were prepared in 100 ml flask containing 5 ml of LB-medium supplemented with Kanamycin. This culture was then diluted with LB + Kanamycin resulting in 50 ml bacteria suspension that was incubated for 4 h at 30 °C. The bacteria were pelleted by centrifugation for 15 min at 3900 g at room temperature and re-suspended in 5 % sucrose solution to get an OD 600 nm (OD_{600}) of 2. After that the suspension was diluted 1:20 with sucrose solution again. Small holes were pierced in the leaves of 4-week-old tobacco plants. The suspension was infiltrated with a syringe with a flat tip until one leave section was completely infiltrated. The leaves were then cleaned thoroughly using a wet tissue. The plants were left for more normal growth conditions in the glass house and observed under the microscope two days later.

2.2.4.5 Stable transformation of Arabidopsis (stable expression)

The overnight cultures from Agrobacteria GV3101 stocks containing the gene of interest were prepared in 200 ml flasks containing 5 ml of LB-medium supplemented with kanamycin, gentamycin and rifampicin. These cultures were then diluted with LB- + Kanamycin medium resulting in 100 ml of bacteria suspension that was incubated for 4-6 h at 30 °C (until an OD_{600} of minimum 0,6 was reached). The bacteria were pelleted by centrifugation for 15 minutes at 4000 g at room temperature and re-suspended in 50 ml 5 % sucrose solution to achieve an OD_{600} of 2. After re-suspending the pellet, the suspension was supplemented with 0.02 % Silwet L-77. The suspension was poured into the square plate and the flowers of the Arabidopsis thaliana were immersed in it. The plants were the wrapped in kitchen foil, incubated at room temperature overnight and the next day unwrapped again, and placed back on the tray in the growth chamber. This floral dipping was repeated a week later to increase the transformation efficiency. Plants were grown until seeds were collected and subjected the segregation analysis.

2.2.4.6 Quantitative detection of Starch degradation

2 ml Eppendorf tubes with two metal balls per tube were prepared. At the end of the day (around sunset) and at the end of the night (around sunrise) around 20-50 mg of leaf material was harvested for every four biological replicates, and immediately froze in liquid nitrogen. The frozen samples were homogenized with the QIAGEN TissueLyser II 4 times at 28 Hz for 1 min each. To the homogenized sample 400 µl 80 % v/v ethanol were added and incubated for

30 min at 80 °C and centrifuged afterwards at 14000 rpm for 10 min. The supernatant was discarded. Next 400 µl of 80 % v/v ethanol were added to the sample and again the samples were incubated at 80 °C for 30 min and afterwards centrifuged at 14000 rpm for 10 min. The supernatant was discarded again. The pellet was suspended in 200 µl 0.5 M NaOH and incubated at 95 °C for 30 min. Then 200 µl (equal volume to NaOH) of 1 M acidic acid were added to each sample. (At this stage the samples can be stored at -20 °C for further processing. From this solution 100 µl have been transferred to a new 1.5 ml Eppendorf tube and 100 µl of fresh α-amyloglucosidase solution (10 mg/10 ml standard buffer (200 ml 1 M acetic acid, 100 ml 1 M NaOH and 700 ml H_2O)) were added and incubate at 55 °C for 2 h. After that the samples were centrifuged for 5 min at 14000 rpm. From the supernatant 50 µl were added to a new 1.5 ml Eppendorf tube (including 50 µl of glucose calibration standard reaction set ups) and mix with 100 µl of glucose oxidase reagent (30 mg glucose oxidase, 3 mg peroxidase, 100 mg o-dianisidine HCl in 100 ml Tris/glycerol buffer pH 7.0 Tris-glycerol buffer: 61 g Tris, + 85 ml 5 M HCl, 255 ml H_2O and 660 ml glycerol)). The mixture was incubated for 1 h at 30 °C. To stop the reaction 200 µl of 5 M HCl were added. The samples were centrifuged at 14000 rpm for 1 min. 200 µl of the supernatant were added to a chamber of a 96-well plate for the measurement and the absorbance of the samples at 540 nm were recorded.

2.2.4.7 Imaging PAM

Using the imaging PAM, the chlorophyll fluorescence of the different plants lines was measured. The measurements were carried under control conditions, after stress treatment and after 7 days of recovery in control conditions. For each measuring on one leaf seven areas were measured simultaneously. For each plant line three biological replicates were measured. For each measurement, the effective quantum yield Y(II), the non-photochemical quenching Y(NPQ) and the proportion of non-regulated energy dissipation Y(NO) were measured at increasingly stronger light intensities (table 1) for 20 s incubation.

Table 1: Incubation time of PAR values for Imaging PAM measurement.

PAR	Inkubation time
0	30 s
2	30 s
22	30 s
42	30 s

58	30 s
104	30 s
135	30 s
206	30 s
299	30 s
582	30 s
727	30 s
924	30 s
1177	30 s
1467	30 s

2.2.4.8 Confocal microscopy

Confocal microscopy of tobacco

The tobacco leaf samples were infiltrated with water using 50ml syringe (Braun) to remove the air in order to improve optical properties of the sample. The sample was mounted on a glass slide, covered with cover glass fixed by a double-sided tape. The confocal microscope (Leica) was used to perform all microscopy imaging with simultaneous acquisition of bright field, CFP/YFP and chlorophyll channels. Following settings were used for detection:

- CFP: excitation UV laser, 30%power; emission detected in the range 460-490nm
- YFP: excitation 514nm argon laser, 30% power; emission detected in the range 520-550nm
- chlorophyll: excitation 514nm argon laser, 30% power; emission detected in the range 630-750nm

Obtained images were analysed by ImageJ software.

Confocal microscopy of tobacco

The Arabidopsis leaf samples were infiltrated with a 40 mM Sucrose solution for stromule induction using 50ml syringe (Braun) to remove the air in order to improve optical properties of the sample. To test the impact of Ca^{2+} on the stromule formation 2 mM Ca^{2+} or 2 mM EGTA was added to the sucrose solution. The sample was mounted on a glass slide, covered with cover glass fixed by a double-sided tape. The confocal microscope (Zeiss LSM 980) was used to

perform microscopy imaging using the Airyscan mode for z-stack imaging. Following settings were used for detection:

- CFP: excitation UV laser, 30%power; emission detected in the range 460-490nm
- YFP: excitation 514nm argon laser, 30% power; emission detected in the range 520-550nm
- chlorophyll: excitation 514nm argon laser, 30% power; emission detected in the range 630-750nm

Obtained images were analyzed by the ImageJ software. The stromule counting was performed using the MiToBo cell counter Plug-in. Instructions were taken from their website. (https://mitobo.informatik.uni-halle.de/index.php/Applications/MTBCellCounter).

3 Results and Discussion

3.1 Impact of OEF18 on abiotic stress conditions

3.1.1 Results – Impact of OEF18 on abiotic stress conditions

3.1.1 1Carbon & Nitrogen starvation and Bortezomib treatment – Growth assay

First of all, growth assays in liquid media have been established. Carbon starvation, and Nitrogen starvation have been simulated to induce autophagy processes to recycle cell material. With this the involvement of OEF18 in such processes was tested. In this first experiment the *oef18/oef18l* double knockout line, was compared with the wildtype, the OEF18 EF-hand mutants, the OEF18-Strep overexpression line and the *atg5* knockout as a positive control for strongly impaired autophagy processes. Additionally, to the starvation processes, a bortezomib treatment has been carried out. Bortezomib is a proteasome inhibitor, inhibiting the 26S proteasome, which is responsible for degrading ubiquitinated proteins in the ubiquitin-proteasome system (UPS). When the 26 S proteasome is inhibited, the autophagy machinery kicks in as an alternative pathway to degrade proteins or organelles and acts as a compensatory mechanism to prevent toxic protein aggregation and maintain cellular homeostasis.

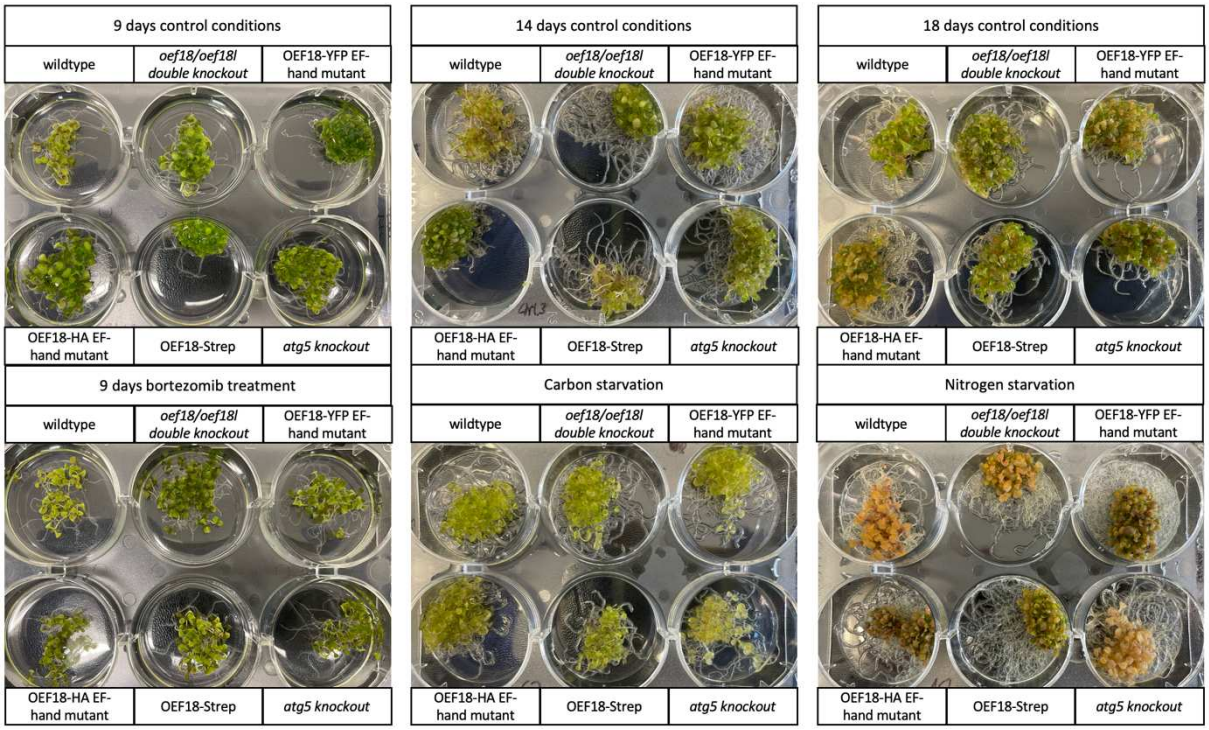

Figure 3: Growth assay in liquid media. The top 3 pictures show the control conditions containing control media and seedlings grown for 9, 14 and 18 days under control conditions. The top middle seedlings were kept in darkness for 5 days after 9 days of growth in light. The lower pictures show the stress treatments. Bottom left seedlings were grown for nine days in control media treated with Bortezomib. Bottom middle seedlings were grown for 9 days in control media and then transferred to C-starvation media kept in dark for 5 days in. Bottom right seedlings were grown for 9 days in control media and then transferred to N-starvation media and grown for 9 several days under control conditions.

The nine days of Bortezomib treatment showed slightly darkened leaves of the *oef18/oef18l* double knockout line, the OEF18-HA EF-hand mutation and the *atg5* knockout line compared to their corresponding controls. The OEF18-YFP EF-hand mutation line, as well as the OEF18-Strep overexpression line showed paler phenotype compared to their corresponding controls. The wildtype showed a pale phenotype in the control condition and after the bortezomib treatment.

After the carbon starvation treatment only the *atg5* knockout plant showed a pale phenotype compared to the other lines of the carbon starvation treatment and their corresponding controls. After the nitrogen starvation assay all the plant lines showed a brownish phenotype. However, both EF hand mutants and the overexpression still showed some greenish parts. To exclude that the observed phenotypes resulted through the stress the plants got through being covered in water, the bortezomib treatment and the nitrogen starvation treatment was established on agar plates. Because no differences were seen during the carbon starvation this starvation treatment was not followed further.

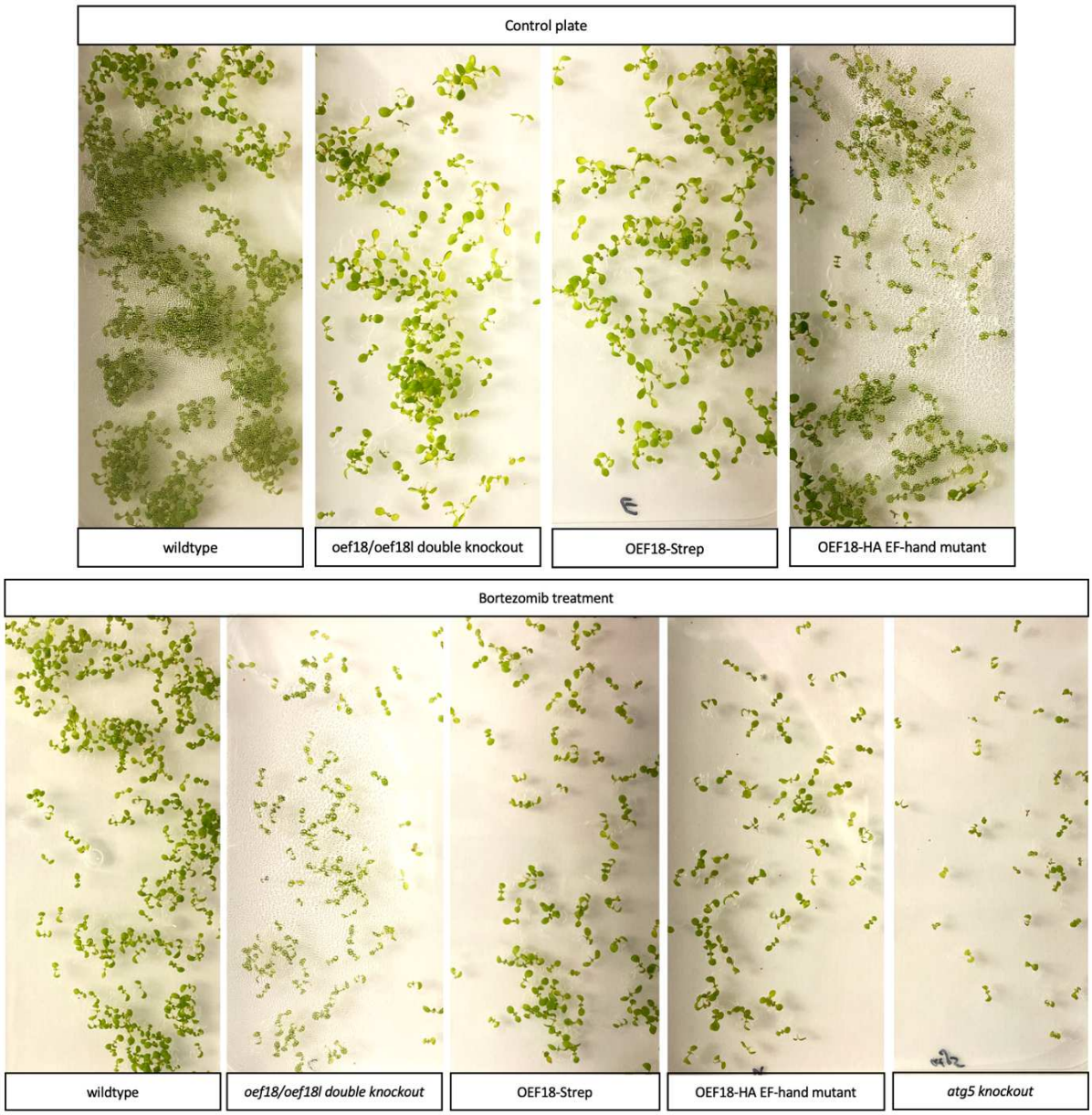

Figure 4: Top. Plant-agar Control plate, bottom: Plant-agar plate treated with 3.75 µM bortezomib, both grown for 9 days under control conditions.

The Bortezomib treatment showed, that *atg5* knockout plants showed a smaller phenotype and half of the seedlings with paler green color. Unfortunately, there was no seedlings left for a control condition. The remaining plants did not show a huge phenotypic difference compared to the wildtype.

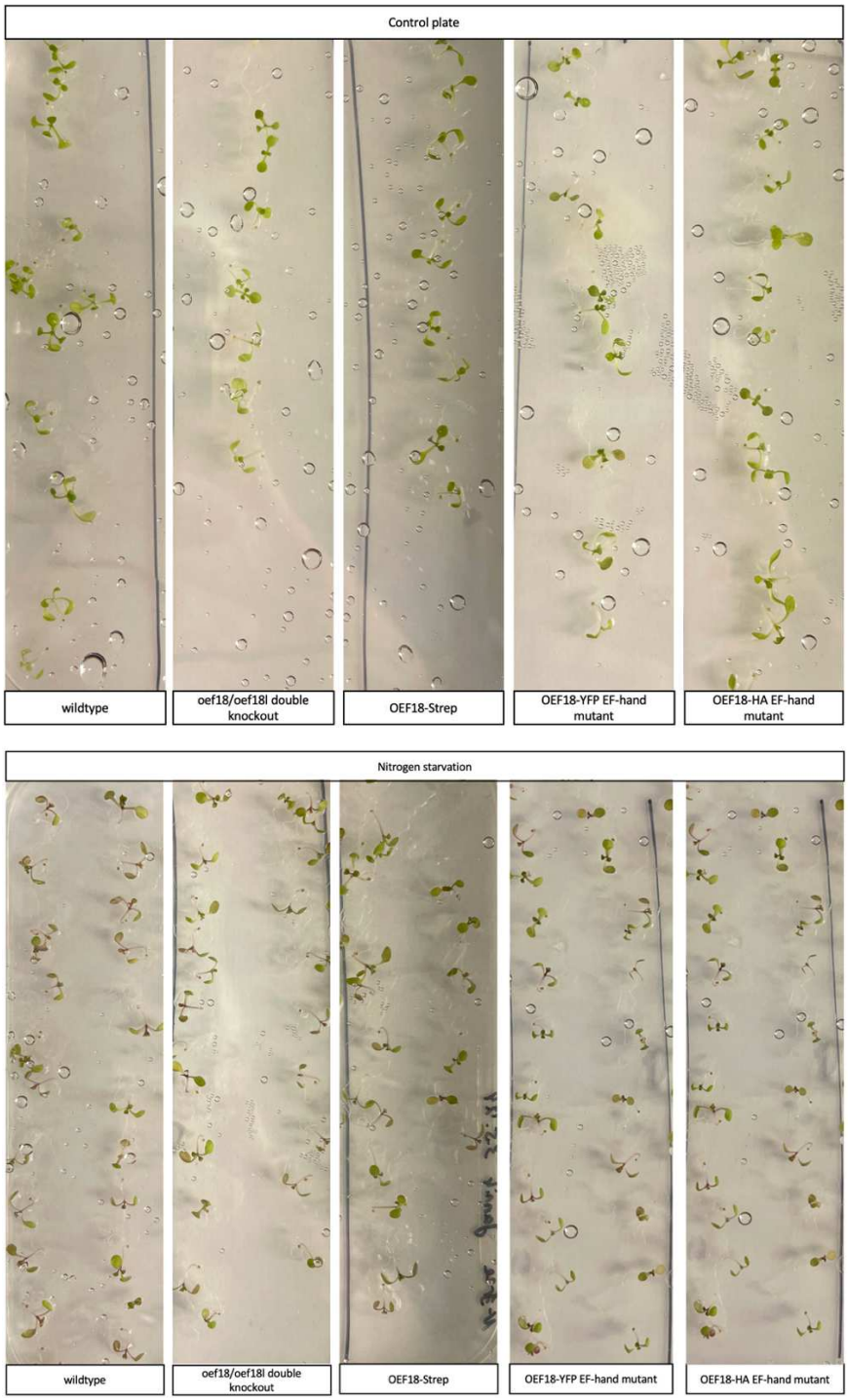

Figure 5: Top: control (growth media) plate, containing seedlings transferred after 3 days of growing from a growth media containing agar plate, grown for 9 more days under control conditions. Bottom: Nitrogen deficient agar plate containing seedlings transferred after 3 days of growing from a growth media containing agar plate grown for 9 more days under control conditions.

The Nitrogen starvation assays showed similar results compared to the bortezomib treatment. All plants showed effects of nitrogen starvation as they showed darkened leaves, which could be an anthocyanin accumulatio, but they did not differ in their phenotype. The control was performed to make sure, the resulting phenotype on the nitrogen starvation plate wasn't a result of the transferring of the 3-day old plants to anther plate.

3.1.1.2 High light & Heat stress – Growth assay

The carbon and nitrogen starvation assays, as well as the bortezomib treatment didn´t show different phenotypes of *oef18/oef18l* double knockout or its EF-hand mutants, which more or less leads to the result, that OEF18 is not involved in a chloroplast recycling process due to starvation. However, OEF18 can still be involved in other stress induced autophagic processes like heat stress or highlight stress. For this 1-week-old Seedlings grown under control conditions (22°C, 150 µE) on agar plates have been exposed to heat stress (37°C) or high light (600 µE) for three days, and observed after another 7 days of recovery under control conditions. Additionally, the OEF18-YFP complementation line and the *oef18* single knockout have been observed under high light and heat stress conditions.

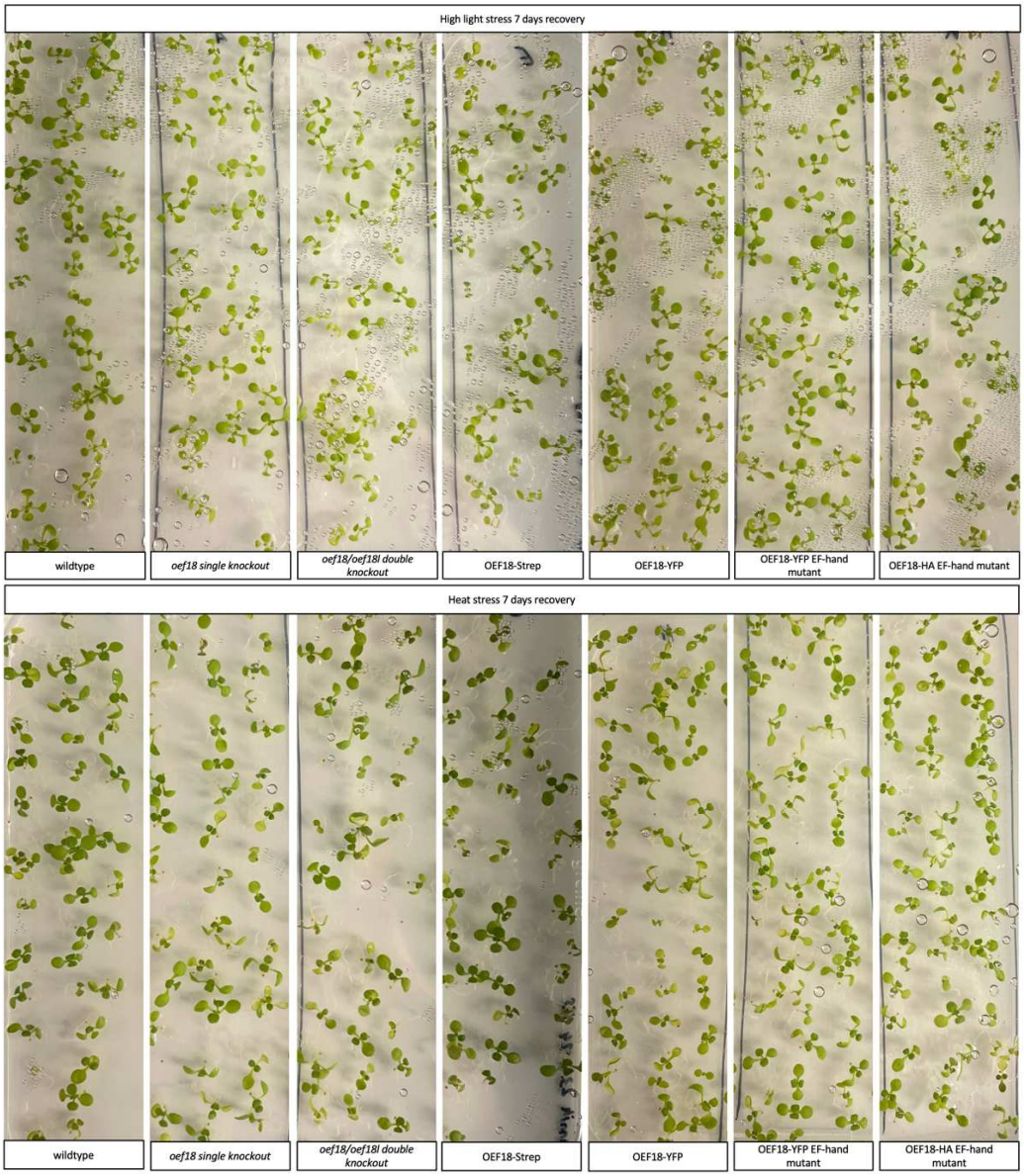

Figure 6: Seedlings on plant agar plates containing growth medium. Exposed to high light (top), or heat stress (bottom) for 3 days. Afterwards, seven days recovery under control conditions.

The high light treatment only showed small phenotypic differences of both *oef18* single knockout and *oef18/oef18l* double knockout compared to the wildtype. The remaining lines did not show any differences compared to the wildtype. The Heat stress treatment showed similar results even though a less promising phenotypic difference of the *oef18* single knockout line and the *oef18/oef18l* double knockout line. However, it cannot be excluded that the observations are mistaken, due to different light angles while taking the picture. Because of this another approach is being established using the Imaging PAM WALZ Mini (referred to later as Imaging PAM).

3.1.1.3 High light and Heat stress – Imaging PAM

Next to the growth assays, Imaging PAM measurements using with 4-week-old plants were established. For this the plants have been tested on their photosynthetic effectivity and their effectivity of photo protection under highlight and heat stress conditions. The Fv/Fm values, the Effective quantum yield of Photosystem II Y(II), the quantum yield of regulated energy dissipation Y(NPQ) and the non-regulated energy dissipation Y(NO), as well as the electron transport rate, from the stress conditions were compared with the control conditions and after 7 days of recovery. First the high light stress was encountered.

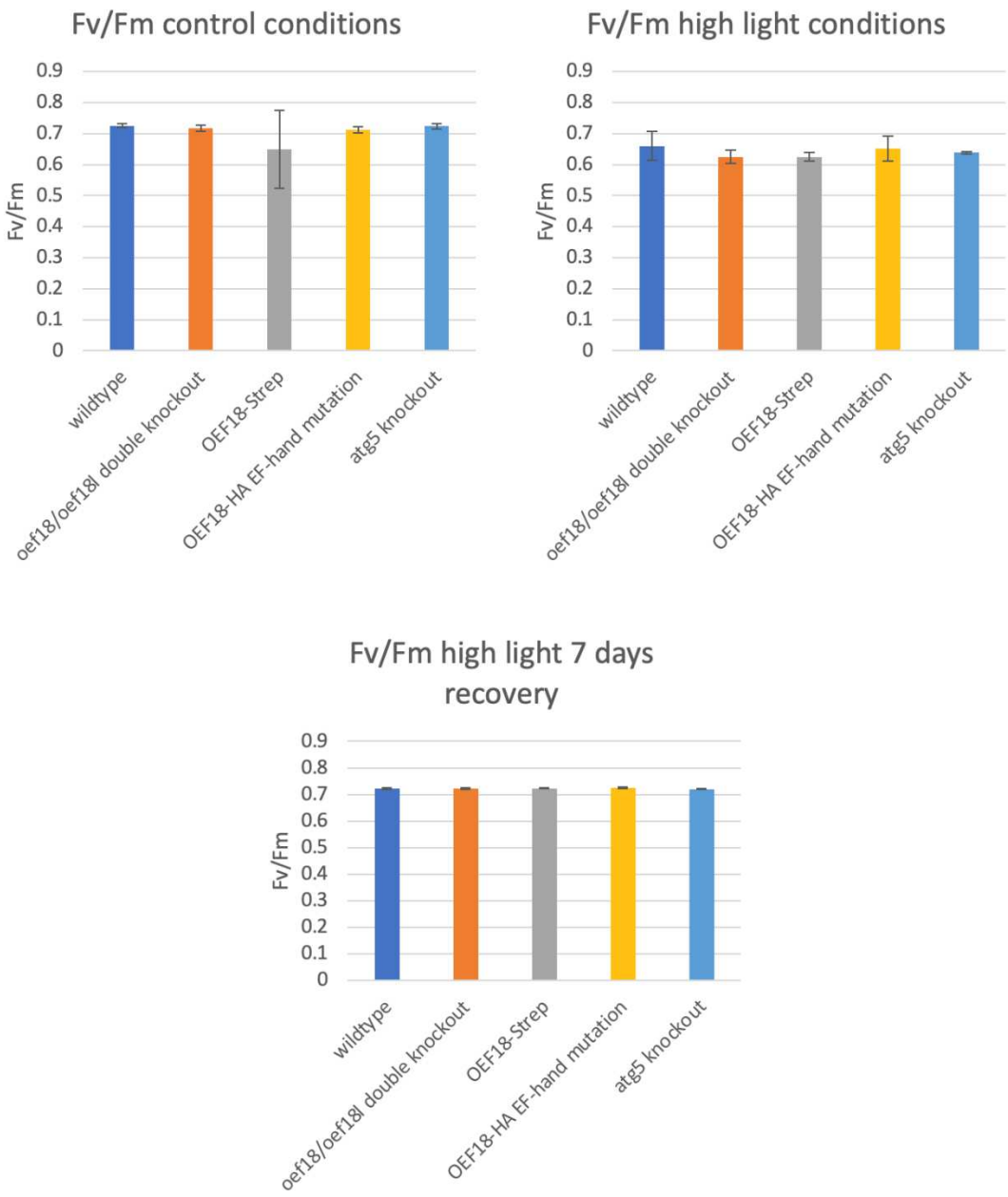

Figure 7: Fv/Fm measurement of control conditions, after 3 days high light treatment and after 7 days recovery under control conditions.

The Fv/Fm of the control conditions before the high-light stress treatment starts are in in the lower optimal region of Arabidopsis plants (0.73-0.83). Except the overexpression line OEF18-Strep shows a reduced Fv/Fm value in the range of 0.65, but because it has quiet high standard deviation it may just be due to an outliner. After 3 days of high light treatment the Fv/Fm values are reduced in all plant lines to around 0.65 to 0.62, indicating that all plants indeed are under stress. Here the double knockout line and the over expression line show the lowest values of 0.62. After 7 days of recovery under normal light conditions the Fv/Fm values are back in the lower optimal region as seen before the high light treatment. Here the OEF18-Strep has a

higher Fv/Fm value indicating that the lower Fv/Fm value from the control conditions indeed was only an outliner.

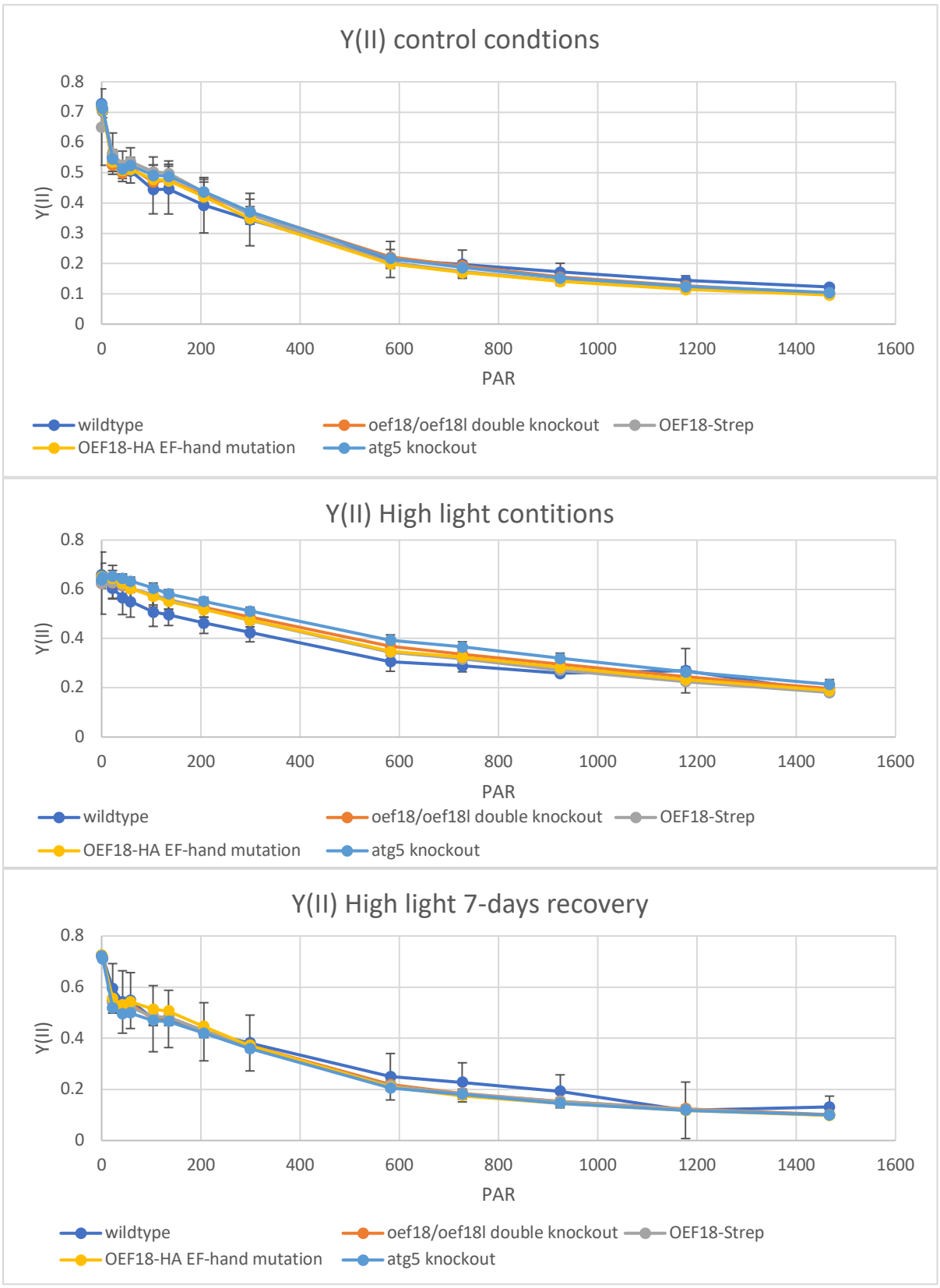

Figure 8: Y(II) measurement of control conditions, after 3 days high light treatment and after 7 days recovery under control conditions.

The effective quantum yield of photosystem II decreases in all three treatments with increasing Photosynthetically Active Radiation (PAR). The control condition showed a slight increasing peak in all lines between PAR values 42 and 58. Here are no recognizable differences between the different plant lines. After three days of high light treatment the Y(II) shows a more or less linear decreasing behavior and there is increasing peak between PAR values 42 and 58. Interestingly the Y(II) values from high light treatment are higher in the high PAR region compared to the control condition. After seven days of recovery under control conditions the Y(II) behaves again as before the stress treatment started. Here again there were no recognizable differences observed between the lines.

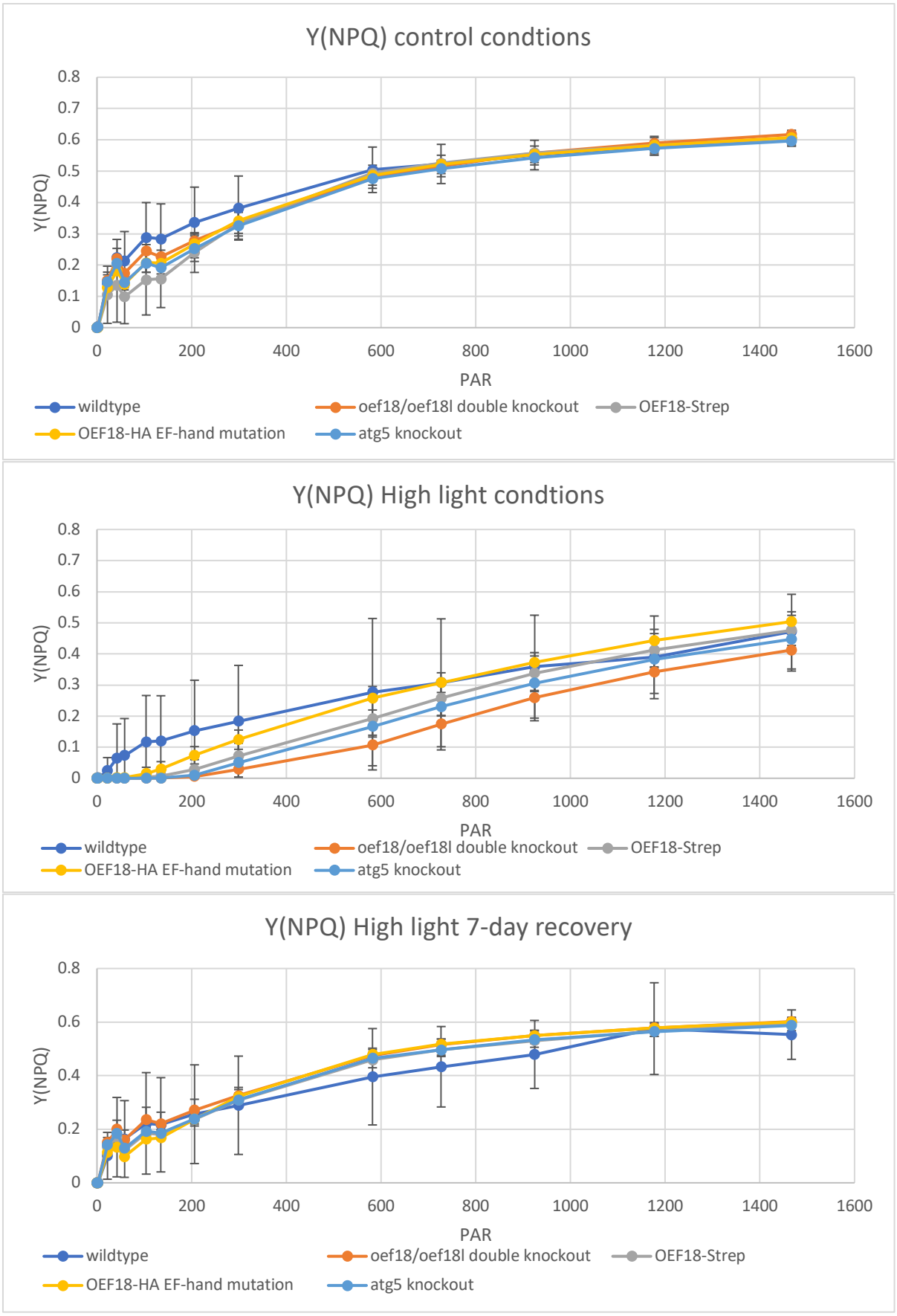

Figure 9: Y(NPQ) measurement of control conditions, after 3 days high light treatment and after 7 days recovery under control conditions.

The quantum yield of regulated energy dissipation increases logarithmic under all three treatments with increasing Photosynthetically Active Radiation (PAR), whereas the control condition and recovery conditions showed logarithmic increasing and the stress treatment showed a more or less linear increasing. The control condition showed a slight decreasing peak in all lines between PAR values 42 and 58. Here are no recognizable differences between the different plant lines. In contrast to Y(II), Y(NPQ) values showed lower Y(NPQ) values after highlight treatment compared to control and recovery conditions. Here they are around 0.2 units lower, whereas the *oef18/oef18l* double knockout showed the lowest value of 0.3 units and the Ef-hand mutant showed the highest value of 0.4 units. After seven days of recovery under control conditions the Y(NPQ) behaves again as before the stress treatment started. Here again there were no recognizable differences observed between the lines.

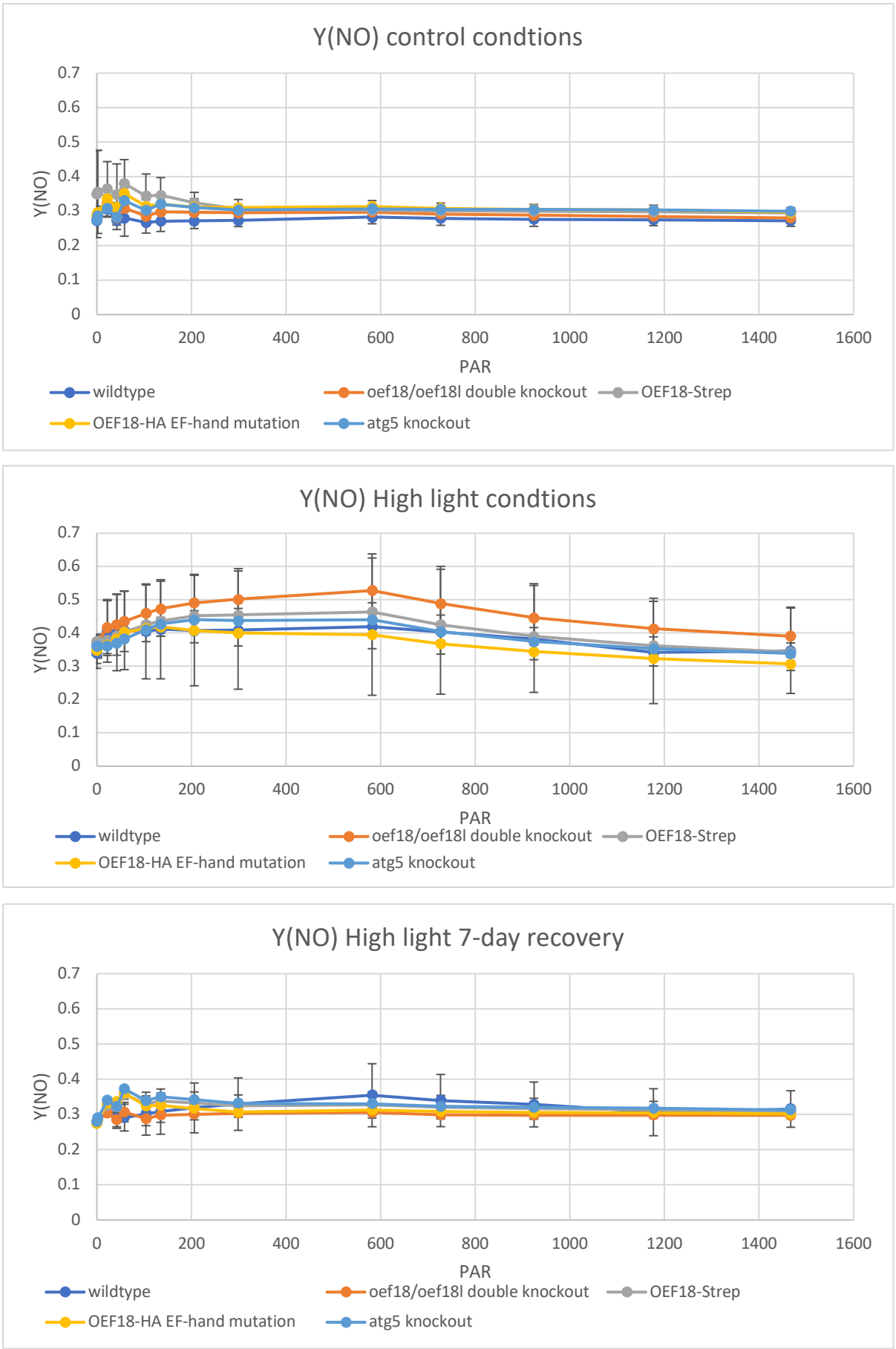

Figure 10: Y(NO) measurement of control conditions, after 3 days high light treatment and after 7 days recovery under control conditions.

The quantum yield of non-regulated energy dissipation of the control conditions and the recovery conditions behaves similar. There is a zigzag behavior in the beginning of the measurement as the Y(NO) increases between PAR value 2-22 from around 0.3 to 0.38, then decreases between 22-42 to 0.4 again, increases between 42 and 58 to 0.38 and decrease again to around 0.3. After that from PAR 206-1400 the Y(NO) value stays around 0.32. Y(NO) of the lines behaves different under the highlight stress conditions. Here the Y(NO) increased between PAR 2-582 and the decreases slowly ending at around 0.34, except the double knockout. *oef18/oef18l* shows a higher non-reregulated energy dissipation having the highest value at PAR 600 (0.53) and then decrease to 0.4 at the end. The Y(NO) of the high light stress treatment is overall increases compared to control and recovery conditions by around 0.1-0.2.

Next to the high light stress a three days heat stress treatment at 37 °C was established. Heat stress often contributes to autophagy because during high temperature there is an over-reduction of the electron transport chain, which leads to an enhanced production of ROS which gives the cell the signal for selective organellar degradation, in this case chlorophagy.
Other contributions of heat stress to chloroplast autophagy processes are the swelling of chloroplasts due to lipid peroxidation and compromise chloroplast membrane integrity, these swollen chloroplasts are often recognized by ATG8-labeled structures and lead to the vacuole (Sieńko *et al.*, 2020). Moreover, Disruption of Photosynthesis, misfolding of proteins and activation of heat-shock proteins and stress responses can contribute to chloroplast degradation.

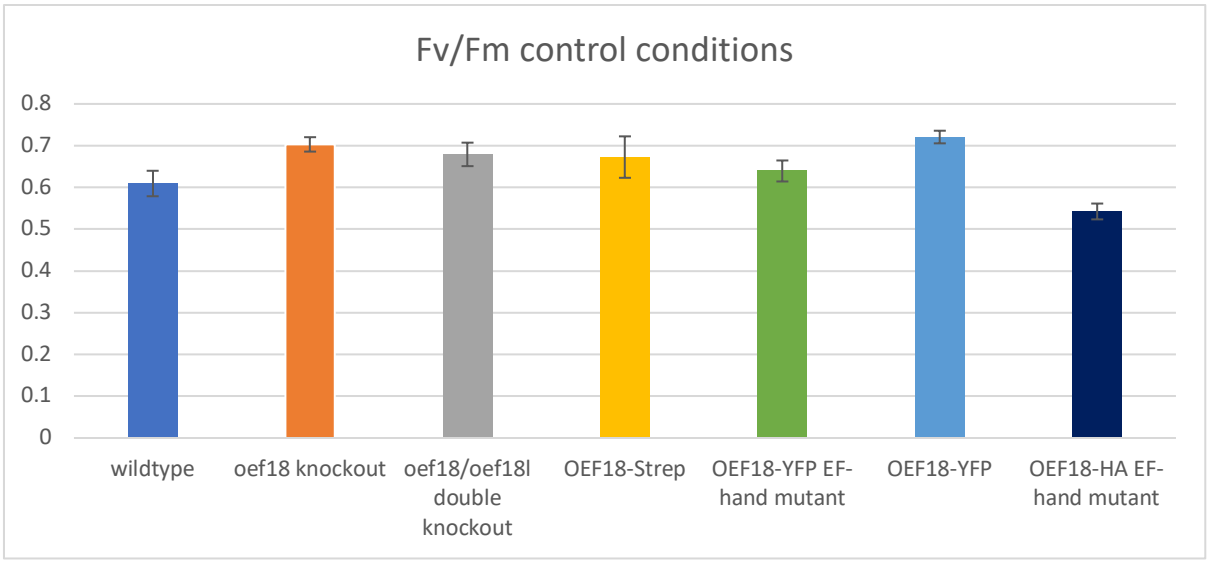

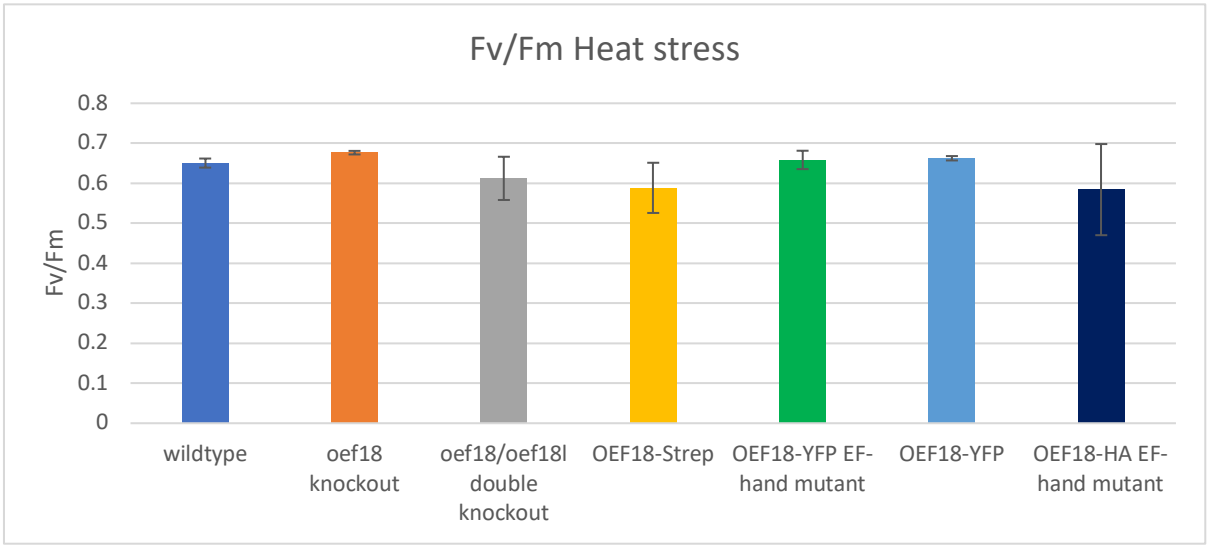

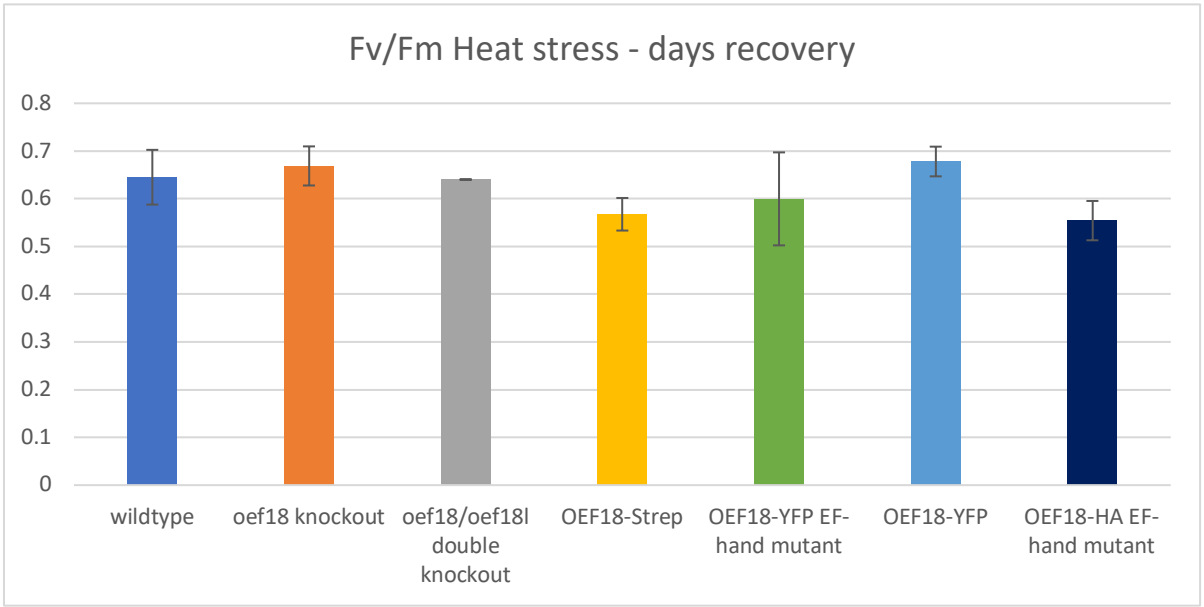

Figure 11: Fv/Fm measurement of control conditions, after 3 days heat stress treatment and after 7 days recovery under control conditions.

The Fv/Fm values of the control conditions are indeed a little low, as the optimal region of Arabidopsis plants is between 0.73 and 0.83. But since only one leaf a plant was measured it still can be, that a weak leaf has been measured. Interestingly the OEF18-HA EF-hand mutant showed the lowest Fv/Fm values under control conditions with a value of around 0.55, followed by the wildtype with 0.6. The fittest plants shown here are the *oef18* single knockout an, *oe18/oef18l* double knockout and the OEF18-YFP line which had a Fv/Fm value of around 0.7- 0.72, which is just below the optimal range. After three days of Heat stress treatment did not show a reduction of all Fv/Fm values. The wildtype, and both EF-hand mutants showed a slightly higher Fv/Fm values, albeit the OEF18-HA EF-hand mutant has a very high standard deviation which may be interpreted as an outliner. From those three lines it could be that fitter leaves as compared to the control conditions have been measured. The other plant lines showed a reduction in the Fv/Fm values, whereas the strongest reduction of around 0.1 has been observed from the double knockout line and the OEF18-Strep overexpression line. But here again they both show a high standard deviation, which could be seen as an outliner as well. After recovery from heat stress for seven days the Fv/Fm values didn't show the same level as before then stress treatment started, unlike the high light treatment. The wildtype shows the same level compared to the heat stress measurement, even though it has a higher standard deviation, meaning it could have had a higher value. The single knockout line showed a similar recovery average as under stress conditions, but here again the standard deviation is higher. The double knockout has a slightly higher Fv/Fm value compared to the stress condition and a solid average, even though not the level of the control condition. The overexpression line showed a reduced Fv/Fm value by around 0.02 after seven days of recovery compared to the stress conditions and a solid average with a lower standard deviation. Compared to the control conditions the Fv/Fm value is reduced by 0.1. The OEF18-YFP EF-hand mutation line has the lowest Fv/Fm value after 7 days of recovery compared to its control condition and the stress treatment, but here too, a very high standard deviation indicating that this is due to an outliner. The OEF18-HA EF-hand mutation has the same Fv/Fm level after seven days of recovery compared to its control condition. The OEF18-YFP line has a slightly reduced Fv/Fm level compared to control condition.

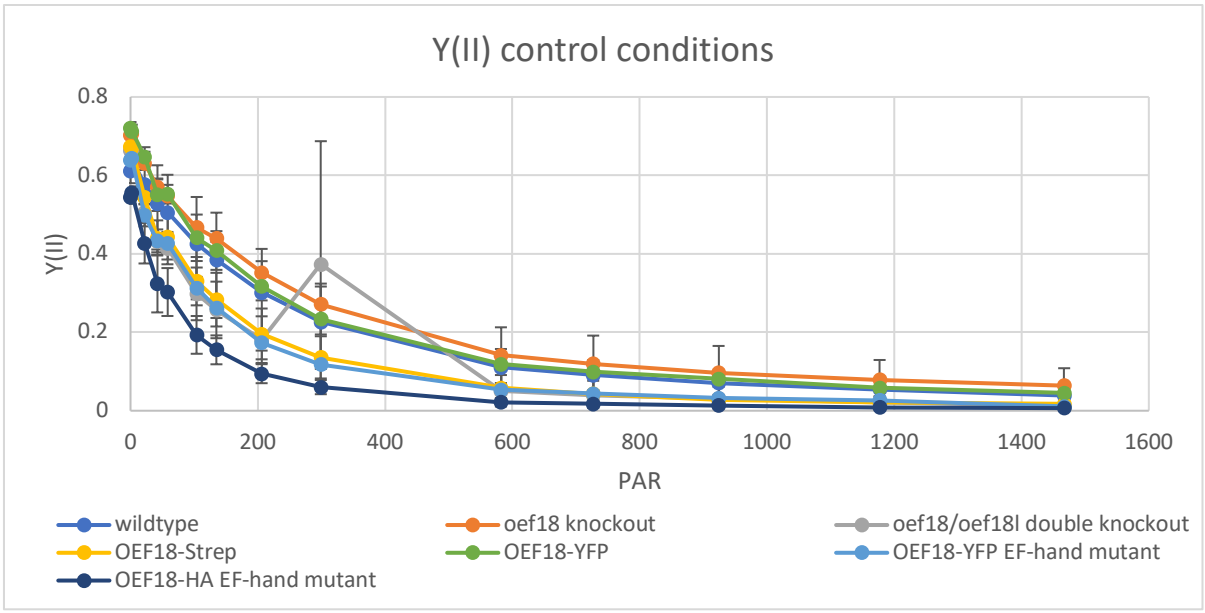

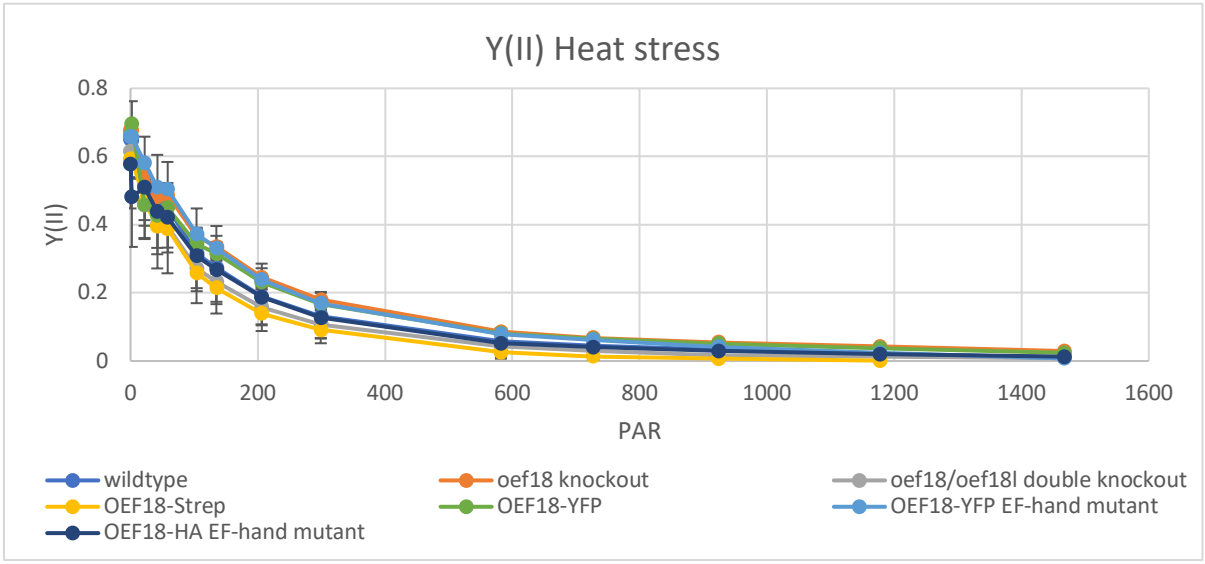

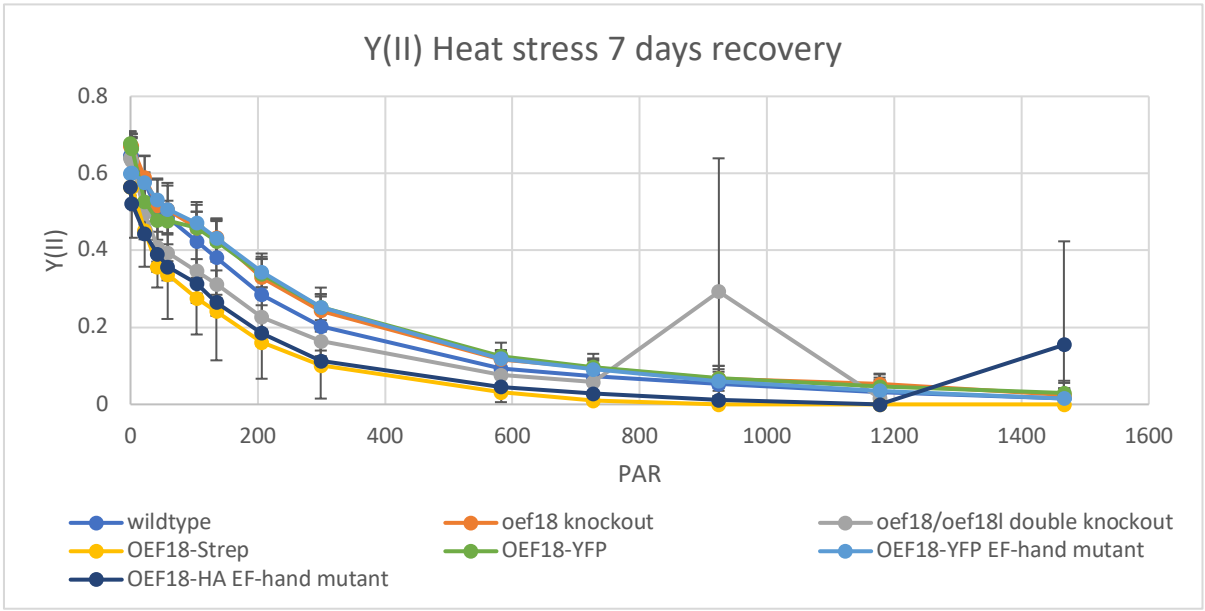

Figure 12: Fv/Fm measurement of control conditions, after 3 days heat stress treatment and after 7 days recovery under control conditions.

The Y(II) from all three treatments behaved globally the same. Between PAR 2-200 the Y(II) decreased strongly by around 0.4-0.5 units and then lowered the decreasing to the end until a value of 0.05 was reached. Under control conditions the OEF18-HA-EF-hand mutant showed the lowest curve showing values of 0.1 units less then overexpression line, the double knockout line and the OEF18-YFP EF-hand mutant line between PAR 2-200. The increased peak of the double knockout line at PAR 299 is considered to be an outliner due to its high standard deviation. The wildtype, the *oef18* single knockout and the OEF18-YFP complementation line showed the highest being 0.2 units higher between PAR 2-200. Under heat stress conditions the dropped overall (except OEF18-HA EF-hand mutant). Here no mentionable differences between the lines have been observed. After seven days of recovery the curves of the different lines went back to the control levels.

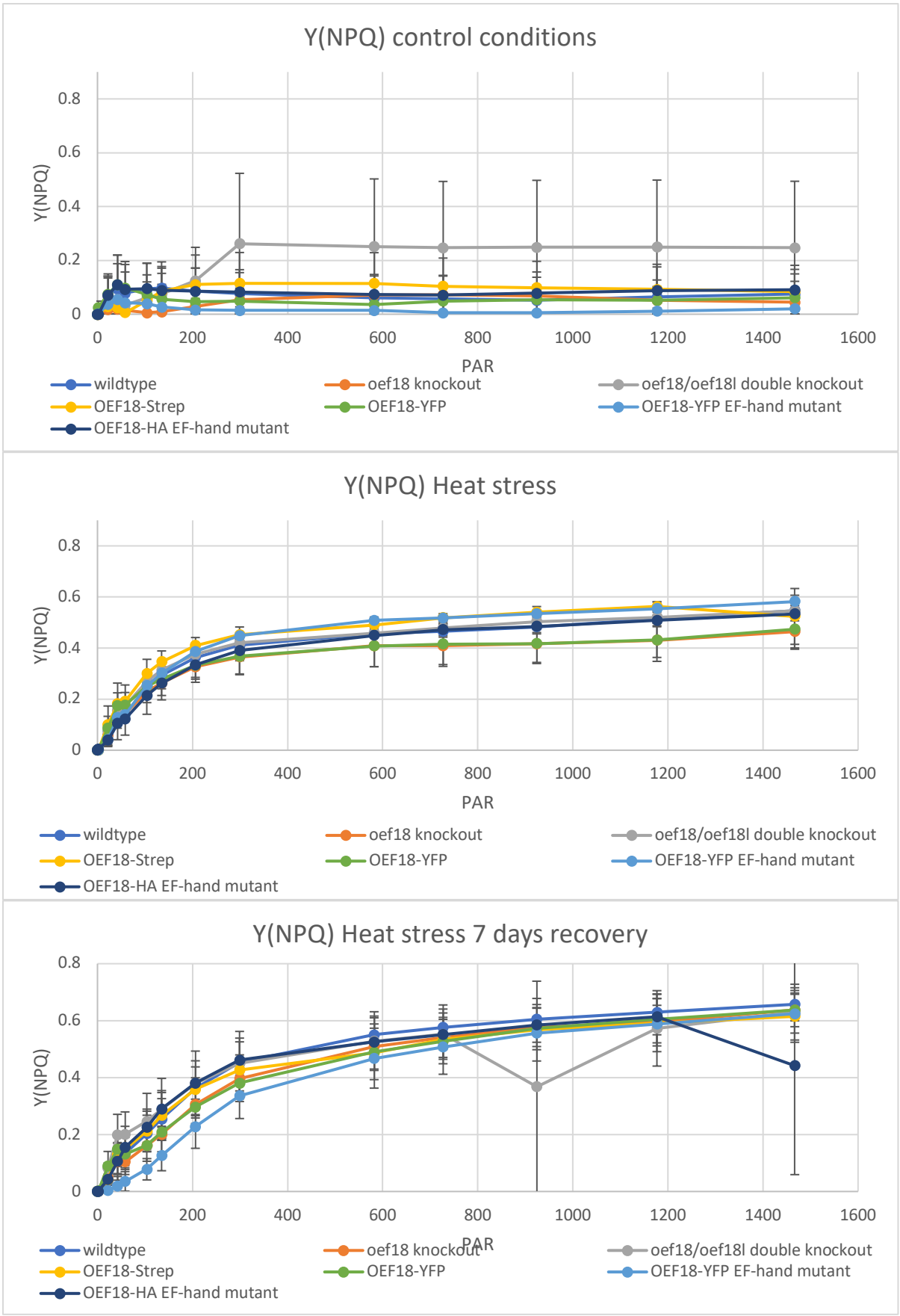

Figure 13: Y(NPQ) measurement of control conditions, after 3 days heat stress treatment and after 7 days recovery under control conditions.

The Y(NPQ) values of the control conditions compared to the control conditions of the high light conditions are very low. Especially the curve of the OEF18-YFP EF-hand mutation line shows very low values, which are close to 0. This would mean, that here is no quantum yield of regulated energy dissipation mearsurable. The curves of the remaining lines accumulated at around 0.1, except the double knockout line having accumulating at around 0.3, which seems to have an outliner leaf. After heat stress treatment the Y(NPQ) rises to rises to around 0.5-0.6, with a strong increasing between PAR 2-200. The *oef18* single knockout line and the OEF18-YFP complementation line showed the lowest curves, being 0.15 lower than the highest curves, being the OEF18-YFP EF-hand mutation and the overexpression line. After seven days of recovery the curves overall increased to 0.65. Globally the curves behaved as the heat stress curves, except two outliners from the double knockout and the OEF18-HA EF-hand mutation.

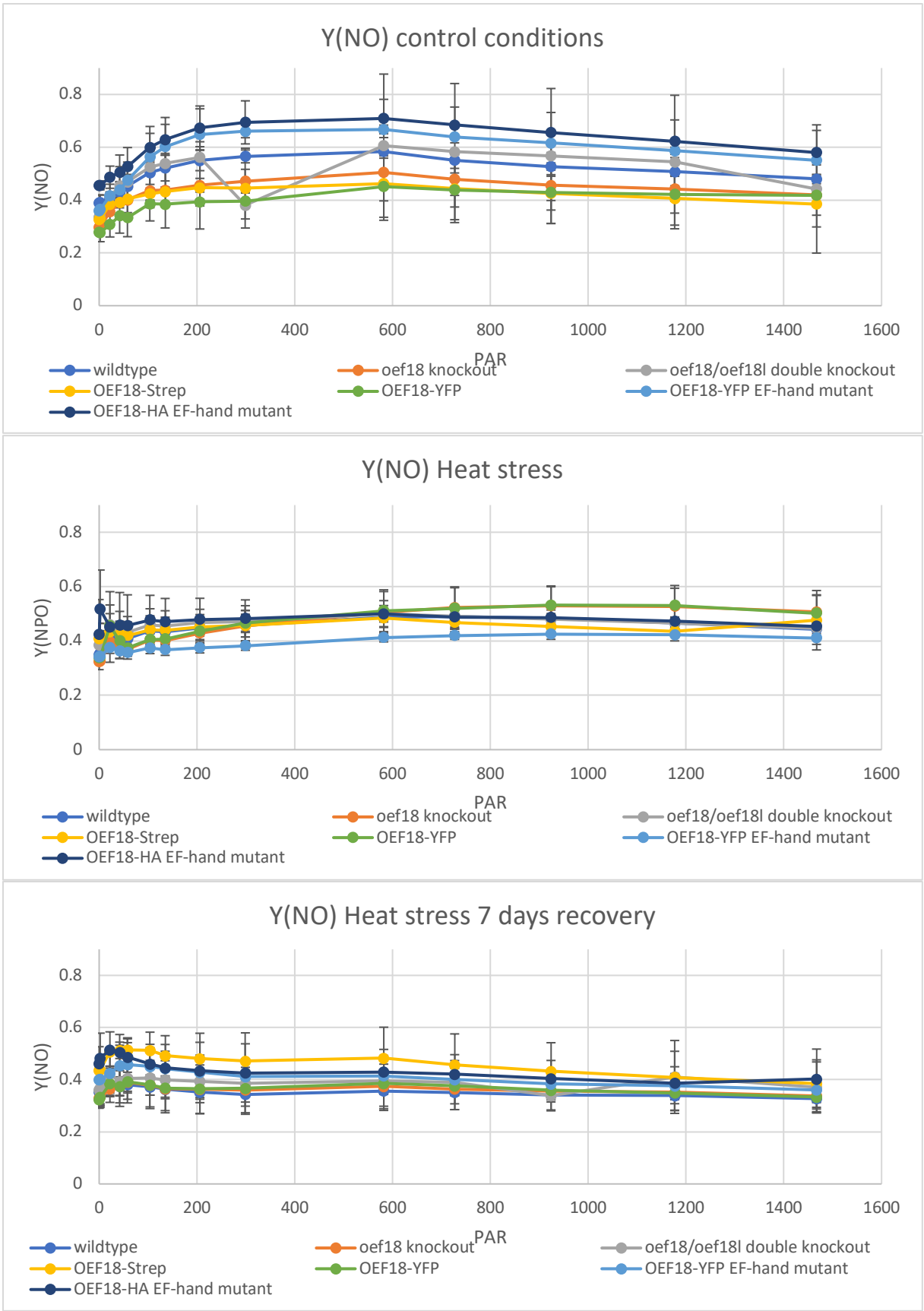

Figure 14: Y(NO) measurement of control conditions, after 3 days heat stress treatment and after 7 days recovery under control conditions.

The non-regulated enegery dissipation of the control condition quite high compared to the control conditions from the high light treatment. But it would fit to the very low regulated energy dissipation values from the heat stress control condition. Especially the wildtype, the doube knockout and the two EF-hand mutation lines have very Y(NO) values (ignoring the outliner from the double knockout) between 0.6 and 0.5 at the end of the measurement and highest values of up to 0.8 at PAR 582. The oef18 single knockout line, the overxpression and the OEF18-YFP complementation line have more moderate values at around 0.4 (but still hiugh compared to the high light control conditions. After the heat stress the the curves from all lines accumulate at around 0.5, except the OEF18-YFP EF-hand mutation being around 0.4. After seven days of heat stress recovery the curves went back from around 0.5 to around 0.4 units. Only the overexpression line did not recover and remaind with a higher Y(NO) level.

3.1.2 Discussion – Impact of OEF18 abiotic stress conditions

Autophagy impaired plant lines like *atg5* knockout plants suffer a lot during starvation processes like carbon starvation or nitrogen starvation because they cannot rely on the important nutrient recycling pathway which depends on autophagic processes. The absence of ATG5 for example results in a failure to form the ATG12–ATG5-ATG16L1 complex, which is critical for autophagosome maturation. Without this complex, the lipidation of ATG8 does not occur effectively, leading to a significant reduction or complete absence of autophagosomes (Zaffagnini and Martens, 2016; Michaeli *et al.*, 2016).

The possible involvement of OEF18 in this manner would be limited to degradation processes from chloroplasts and peroxisomes, since it is localized in their membranes.

The phenotypes that have been observed in the liquid growth assay of the nitrogen starvation and the bortezomib treatment could not be repeated with the growth assays on agar plates (figure 4 and 5). Hence the brownish phenotype observed at the nitrogen-deficient liquid growth assay (figure 3) of the *oef18/oef18l* double knockout is considered to appear because of the additional stress of the plants being in a liquid medium. Same applies for the paler *oef18/oef18l* double knockout seedlings in the liquid bortezomib treatment (figure 3).

Since the seedlings growth assays did not show any visible phenotypic differences under heat stress and high light conditions between the different lines, the Imaging PAM measurements were established, to take a closer look the of chloroplast health and their potential degradation

in response to stress conditions and the potential impact of OEF18. To confirm an involvement, we would expect to see

- decreased Fv/Fm, indicating potential damage to PSII,
- reduced Y(II) reflecting lower actual PSII efficiency under stress,
- increased Y(NPQ) showing enhanced protective energy dissipation efforts and
- elevated Y(NO) signifying inefficient energy management and possible chloroplast damage

of the *oef18* single knockout line and the *oef18/oef18like* double knockout line. If Ca^{2+} ions would also be involved in this process, we additionally would expect a similar behavior of both EF-hand mutants, compared to the OEF18-functional lines (Baker, 2008; Barbagallo *et al.*, 2003; Maxwell and Johnson, 2000).

The Imaging PAM results overall showed the expected results, meaning decreased Fv/FM, Y(II) and Y(NPQ) and increased Y(NO) values after highlight and heat stress after, which recover after seven days under normal conditions. It also fits that from each measurement the effective quantum yield of PS(II) Y(II) drops with increasing pulse amplitude radiation, whereas the Y(NPQ) Y(NO) increase with increasing PAR. Higher Y(NPQ) under stress conditions implies increased energy dissipation as a protective mechanism. Over time, if photoprotection fails and the stress persists, it may contribute to chloroplast degradation. Y(NO) tends to increase when chloroplasts are damaged and can no longer regulate energy dissipation effectively, a condition that might necessitate chloroplast degradation to prevent further cellular damage (Barbagallo *et al.*, 2003; Baker, 2008).

From the Imaging PAM results of both, the highlight stress and the heat stress conditions, we can exclude the involvement of OEF18 in chloroplast degradation processes, since we do not see decreased Fv/FM, Y(II) and Y(NPQ) or increased Y(NO) values neither of the single or double knockout. Resulting from this, the EF-hand mutation lines can also be ignored in this discussion, since OEF18 has no impact in chloroplast degradation processes.

Albeit the Imaging PAM measuring may be worthy to repeat, with the Imaging PAM Maxi, which can in contrast to the Imaging PAM mini, measure the whole plant, not just one leaf. This would cancel out invalid values from bad leaves, and give a good average between different aged leaves. Considering having not one but 4 plants in one pot, with one measuring 4 plants could be observed giving a higher number of biological replicates, which would also

reduce the impact of possible outliners. Especially under heat stress conditions the outliners made it hard to interpret the results.

3.2 Impact of OEF18 on stromule formation

3.2.1 Results – Impact of OEF18 on stromule formation

To compare chloroplast stromule formation and peroxisome accumulation around chloroplasts of the different plant lines stroma-markers and peroxisome-markers were designed. For this Ribulose-1,5-Bisphosphat-Carboxylase/Oxygenase small subunit (RBCS) was fused with Yellow Fluorescent Protein (YFP) C-terminally as a stroma marker, and Cyan fluorescent protein (CFP) was fused to with the Peroxisome targeting sequence 1 (PTS1) [SKL] C-terminally. The markers have been cloned into the binary pBIB vector backbone containing an sCherry seed code marker (figure 15 A&B). These vectors were transformed into competent *Agrobacterium tumefaciens* cells.

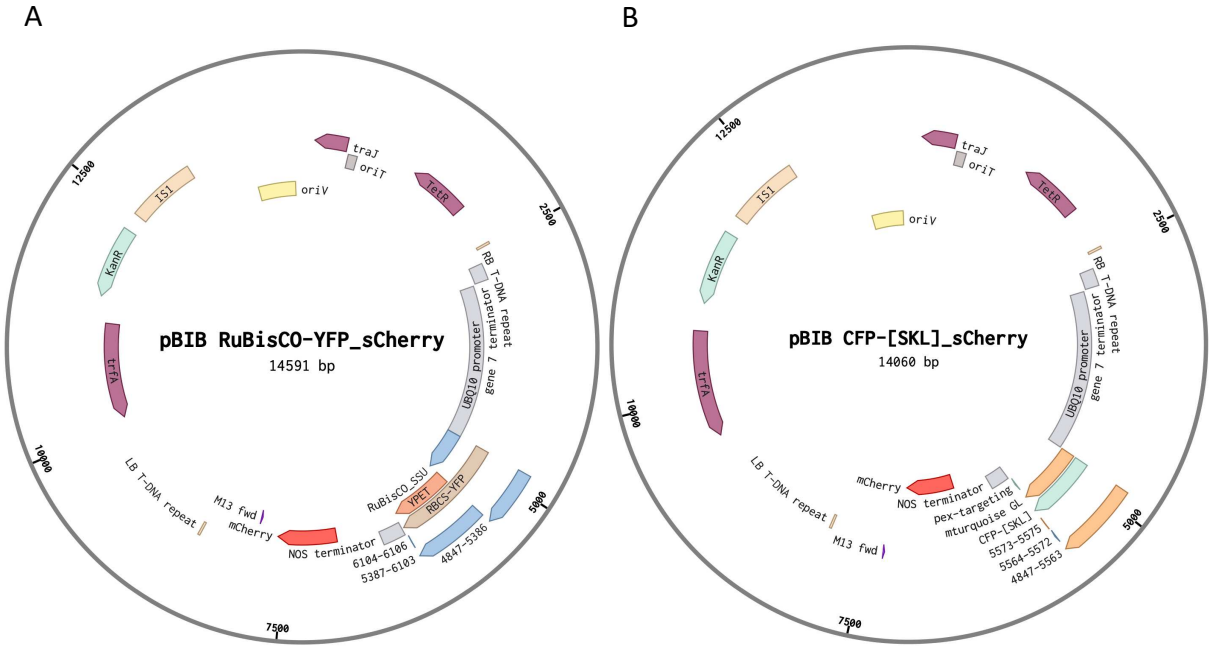

Figure 15: pBIB vectors for agro-infiltration in Nicotiana tabacum and agro-transformation in Arabidopsis thaliana. A) RuBisCO-YFP as a stroma marker in pBIB vector with seed code marker gene. B) CFP-[SKL] as a peroxisome marker in pBIB vector with seed code marker gene.

Before the markers were introduced to Arabidopsis plants, they were tested on their functionality by infiltrating them in tobacco plants (figure 2 and 3). The results in figure 2 & 3 showed that both the stroma marker and the peroxisome marker are functional as RBCS-YFP is only located to chloroplast stroma and CFP-[SKL] is only located in the peroxisomes.

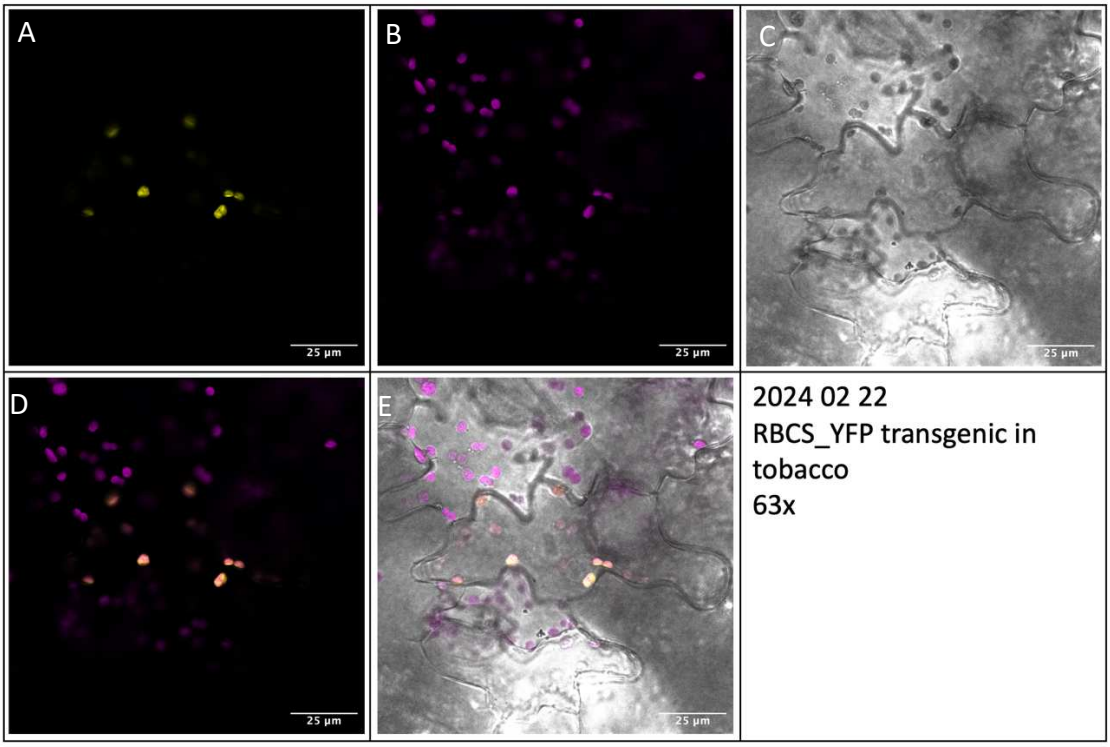

Figure 16: Microscope image with confocal microscope (Leica) of tobacco leaf infiltrated with competent *A. tumefaciens* cells containing the RBCS-YFP stroma marker in 63x magnification. A) RBCS-YFP marking chloroplast stroma. B) Chlorophyll autofluorescence showing the chloroplasts. C) brightfield illumination. D) merge of A and B. E) merge of A, B, and C.

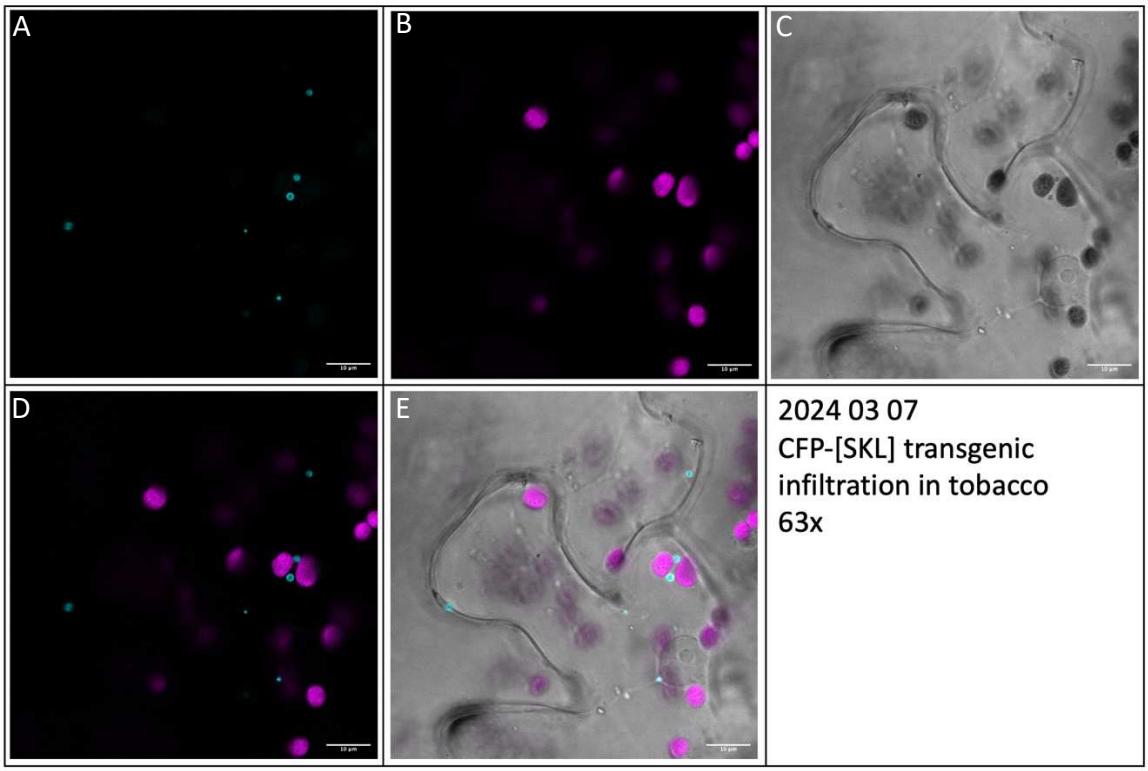

Figure 17: Microscope image with confocal microscope (Leica) of tobacco leaf infiltrated with competent *A. tumefaciens* cells containing the CFP-[SKL] peroxisome marker in 63x magnification. A) CFP-[SKL] marking peroxisomes. B) Chlorophyll autofluorescence showing the chloroplasts. C) brightfield illumination. D) merge of A and B. E) merge of A, B, and C.

Since the functionality of the two markers was given, Arabidopsis thaliana lines have been dipped with competent Agrobacteria containing these markers to get stable lines. Successful transformed seeds were picked as they showed red fluorescence as they were excited.
Unfortunately, the peroxisome marker has not been functional in all dipped Arabidopsis lines, even though the seeds harvested from dipped Arabidopsis plants showed red fluorescence due to the sCherry seed-code marker and the reverse transcriptase PCR measurement of the lines showed that the peroxisome marker is expressed (supplementary figure 1). Why the peroxisome marker is unfunctional in all the transformed lines is still unresolved, since the CFP fused with the PTS1 [SKL] was functional in transformed Arabidopsis plants in the dissertation of Dr. Przemyslaw Kmiecik Due to this, the peroxisome accumulation to chloroplasts and OEF18's involvement in the possible communication between theses organelles cannot be compared between the *oef18/oef18l* double knockout line and the wildtype and the OEF18-Strep overexpression line.
On the other hand, the RBCS-YFP marker has been functional in dipped Arabidopsis leaves, therefore the involvement of OEF18 in stromule formation and the impact of calcium in this manner can still be discussed (figure 4). For this the leave samples have been vacuum-infiltrated with artificial pond water to observe the stromule formation under normal conditions. Additionally, the leave samples have been observed after vacuum infiltration with APW supplied with a 40 mM sucrose solution in artificial pond water (APW) and incubation in darkness for 2 h to induce the chloroplast stromule formation according to (Schattat and Klösgen, 2011).

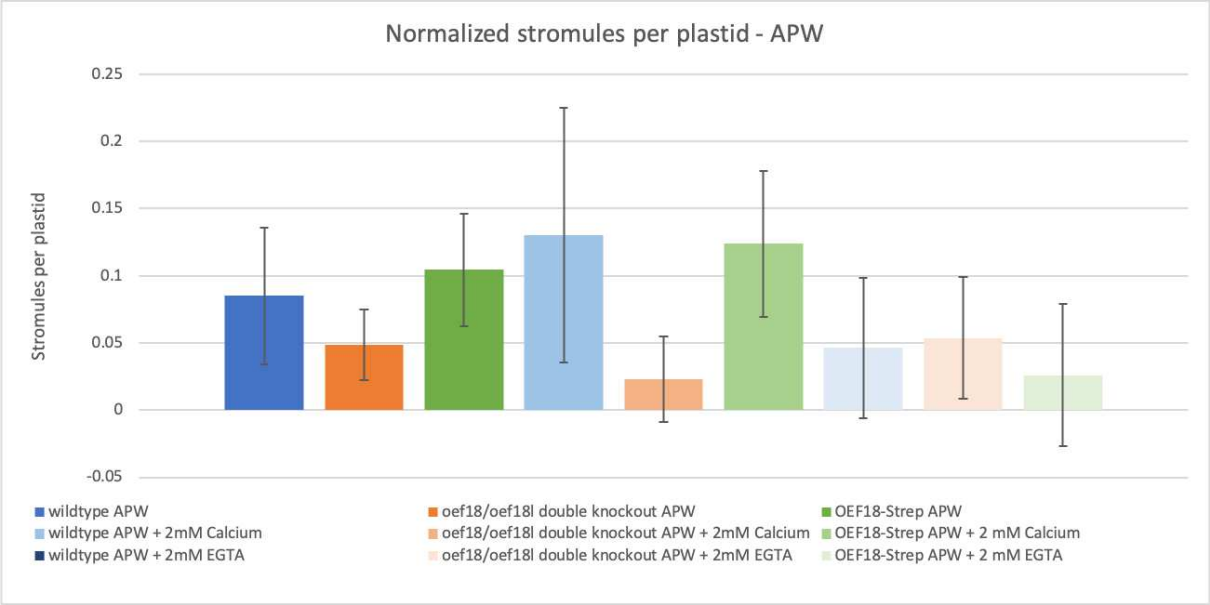

Figure 18: Amount of stromules normalized to the number of plastids of 4-week-old Arabidopsis leaves of wildtype, *oef18/oef18l* double knockout and OEF18-Strep overexpression vacuum infiltrated with either artificial pond water, additionally supplied with 2 mM Calcium or supplied with 2 mM Ethylenglycolbis(aminoethylether)-N,N,N′,N′-tetraessigsäure (EGTA).

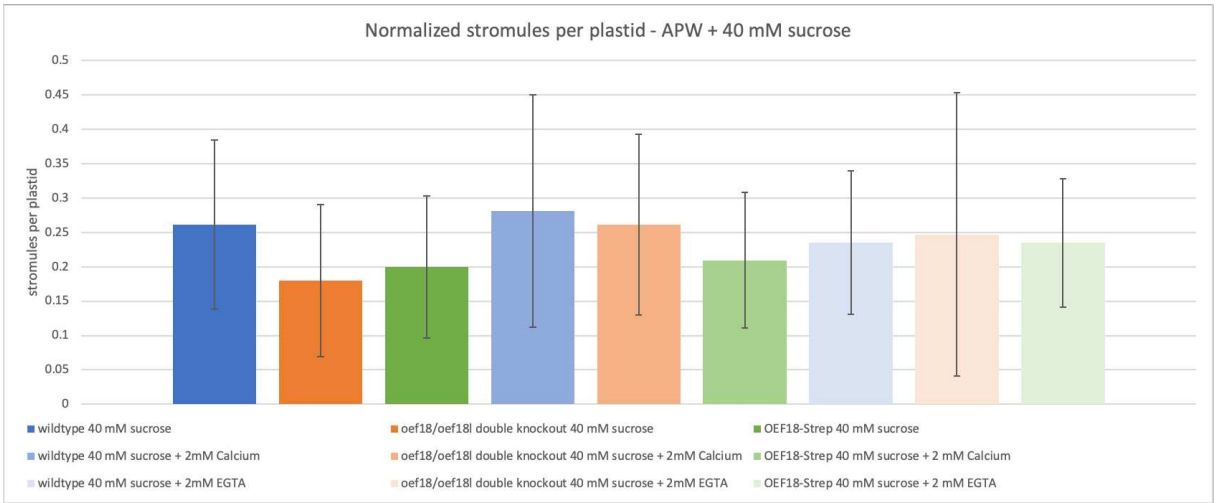

Figure 19: Amount of stromules normalized to the number of plastids of 4-week-old Arabidopsis leaves of wildtype, *oef18/oef18l* double knockout and OEF18-Strep overexpression line vacuum infiltrated and incubated for 2 hours in darkness in either only 40 mM Sucrose solution, additionally supplied with 2 mM Calcium or supplied with 2 mM Ethylenglycolbis(aminoethylether)-N,N,N′,N′-tetraessigsäure (EGTA).

The results from figure 18 indicate that OEF18 may have an indirect effect on stromule formation. When incubated with artificial pond water (APW) alone, the wild-type plants showed a stromule frequency of approximately 8% per plastid. In contrast, the *oef18/oef18l* double knockout exhibited a reduced stromule frequency of about 5%, while the OEF18 overexpression line showed an increased frequency of around 10%. When 2 mM calcium ions were added to the APW, stromule formation was significantly enhanced in the wild-type and

OEF18 overexpression lines, with both showing an increase to approximately 13% of the observed plastids. However, the double knockout line exhibited a sharp decrease in stromule formation, dropping to around 2.5%. When 2 mM EGTA (a calcium chelator) was added to the APW, the stromule formation was suppressed in the wild-type and OEF18 overexpression lines, with a frequency reduced to 5% and 2.5%, respectively. Interestingly, the double knockout line remained unchanged at 5% stromule frequency under these conditions.

In experiments where APW was supplemented with sucrose to artificially induce the stromule formation, the wild-type plants displayed a significant increase in stromule formation, with the frequency rising to 25%. The double knockout line exhibited a reduced frequency of 18%, while the OEF18 overexpression line showed a moderate increase, reaching 20%. When 2 mM calcium was added to the sucrose solution, the wild-type further increased its stromule frequency to 28%. However, in the double knockout line, the addition of calcium caused a marked rise in stromule formation, reaching 45% compared to the sucrose-only treatment. The OEF18 overexpression line did not show any significant changes with calcium addition, maintaining the same stromule frequency as in the sucrose-only condition. Finally, the addition of 2 mM EGTA to the sucrose solution had varying effects: stromule formation in the wild-type decreased slightly to 24%, while the double knockout line showed a modest increase to 25%. Similarly, the OEF18 overexpression line also displayed an increase, with stromule frequency rising to 25% in the presence of EGTA.

3.2.1 Discussion – Impact of OEF18 on stromule formation

The objective of this part of the study was to investigate the role of OEF18 in the chloroplast stromule formation and crosstalk between peroxisomes and chloroplasts.

The latter cannot be discussed since the peroxisome marker was unfunctional in Arabidopsis due to unresolved reasons. For this the marker hast be redesigned e.g., with another peroxisome targeting peptide other than [SKL] like [SRL] (Ma and Reumann, 2008; (Anon, 1989). But since the targeting peptide has been used before in microscopy experiments in (Kmiecik, 2018) and was shown functional as it marked peroxisomes exclusively, it is doubtable that the problem is due to the [SKL] targeting peptide.

Despite this, the role of OEF18 in stromule formation could still be analyzed and discussed in depth. If OEF18 positively influences stromule formation, one would expect a decrease in stromule frequency in the *oef18/oef18l* double knockout line compared to the wild-type and

OEF18 overexpression lines. The data from figure 18 support this hypothesis, as the double knockout line exhibited roughly half the stromule frequency observed in the wild-type and overexpression lines under normal conditions, suggesting a clear involvement of OEF18 in stromule formation under control conditions. It should also be noted that the stromules observed in the oef18 double knockout are strongly shortened and usually only recognizable as a bulge in the plastid. To further analyze this a more complex analyzation mode has to be applied, to measure the exact length of stromules.

Calcium ions (Ca^{2+}) were also tested in this experiment due to their well-established role in cellular processes such as signal transduction, cytoskeletal dynamics, and organelle movement within plant cells. Calcium's involvement in regulating stromule formation is particularly intriguing, as it could serve as a secondary messenger in response to environmental or metabolic cues (Stael *et al.*, 2012; Dodd *et al.*, 2010). Consistent with this idea, the addition of 2 mM calcium ions enhanced stromule formation, while calcium chelation with EGTA reduced stromule frequency, underscoring calcium's regulatory role. These findings align with prior research showing that OEF18 can bind calcium under physiological conditions and form tetramers in its presence (Kmiecik, 2018).

The precise mechanism by which OEF18 influences stromule formation remains unclear. One hypothesis is that OEF18 tetramers might form a channel that facilitates the transport of molecules essential for stromule formation. A more prominent possibility is that OEF18 tetramers could act as a scaffold for microtubules, forming part a plastidial linker platforms required for cytoskeletal dynamics. Further research will be necessary to elucidate these potential mechanisms. In chapter 3.4 the tubules are tested on the interaction with OEF18 to give hints of OEF18's role in a microtubule linker.

In the second phase of the experiment, sucrose was added to the artificial pond water (APW) to artificially induce stromule formation and increase the contrast between the experimental conditions. Interestingly, this approach yielded different results. No consistent differences in stromule frequency were observed between the wild-type, knockout, and overexpression lines, and the effects of calcium and EGTA were less pronounced. This suggests that, under sucrose-induced conditions, a different, OEF18-independent mechanism for stromule formation may be activated.

A critical factor to consider in these experiments is the high standard deviation observed in stromule frequency measurements. This variability may stem from biological differences

between leaves. To mitigate these issues, future studies should examine multiple leaves from different Arabidopsis plants to reduce the impact of outliners, as well as leaves having the same age. As suggested by Schattat and Klösgen (2011), high-throughput microscopy methods could improve the consistency and speed of stromule quantification. Additionally, testing other divalent cations like magnesium in future experiments could help determine if the observed effects are specific to calcium or related to general properties of divalent ions.

3.3 Impact of OEF18 on transitory starch degradation

3.3.1 Results – Impact of OEF18 the transitory starch degradation

Next the possible impact of OEF18 in the degradation of transitory starch, as observed in experiments done by Dr. Przemyslaw Kmiecik (figure 2), should be proven. Since the lugol's starch detection experiment is very unreliable, only the enzymatic quantitative starch detection was repeated in this project.

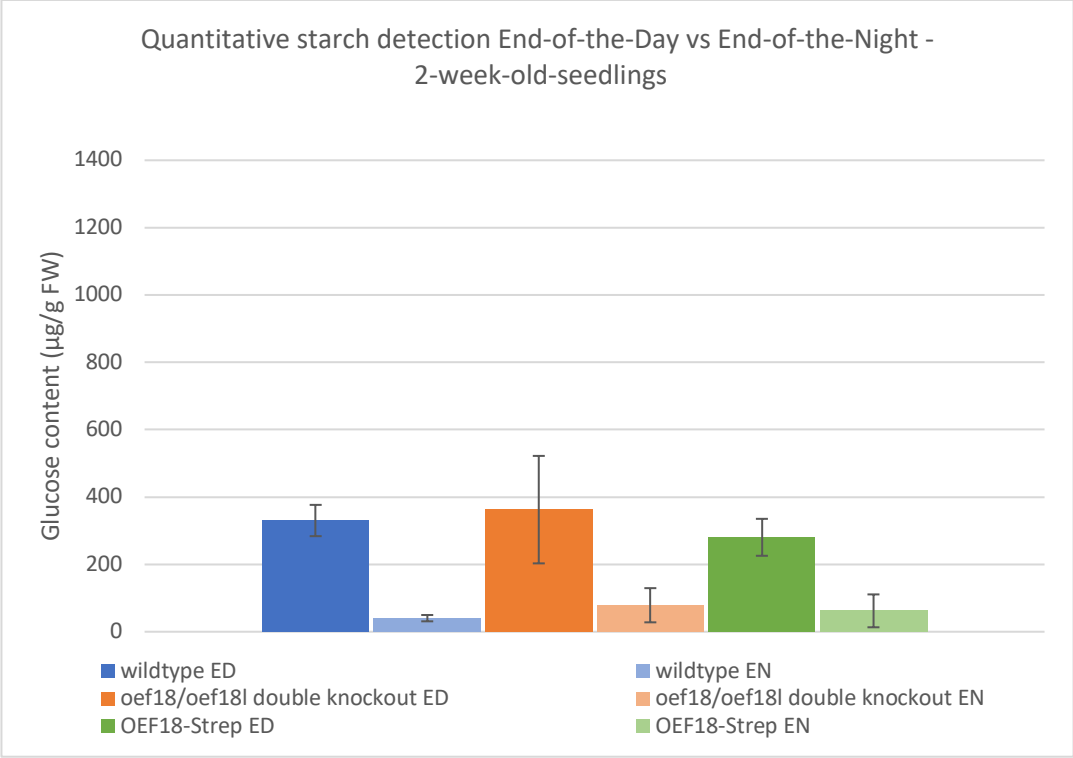

Figure 20: Enzymatic quantitative starch detection assay of 2-week-old wildtype, oef18/oef18l double knockout and the OEF18-Strep overexpression line seedlings at the end of the night and at the end of the day. The glucose content in µg glucose per g fresh-weight (FW) content corresponds to the starch content after the free glucose has been washed out of the leaf material and the remaining starch has been broken down to glucose with beta-glucosidase.

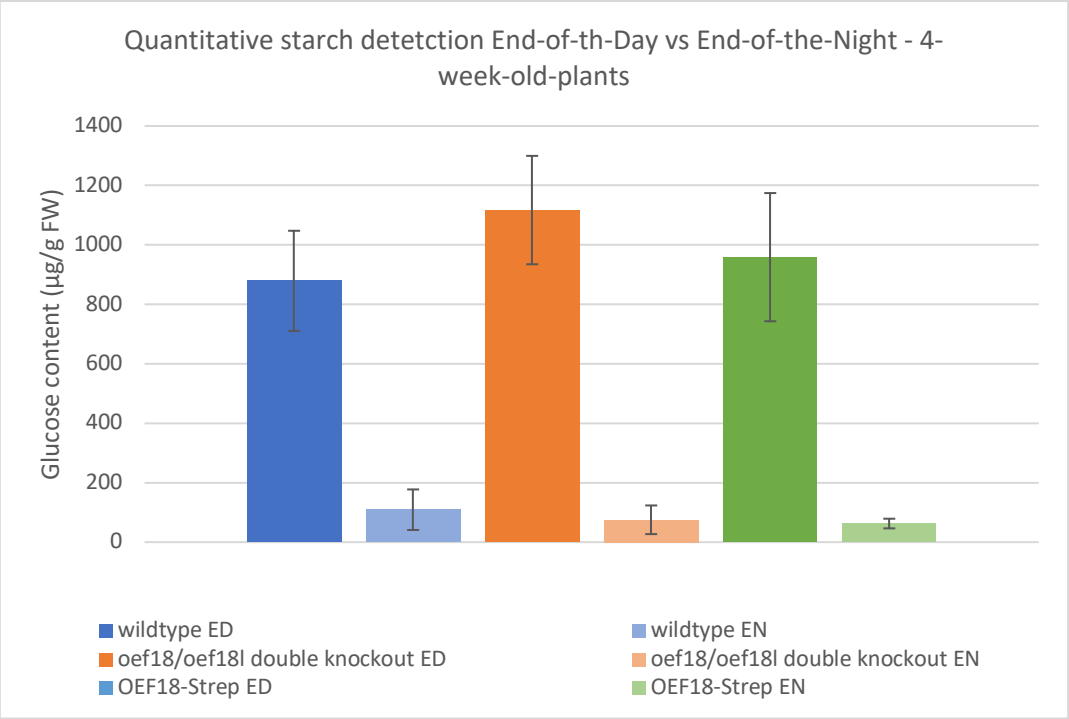

Figure 21: Enzymatic quantitative starch detection assay of 4-week-old wildtype, oef18/oef18l double knockout and the OEF18-Strep overexpression line plants at the end of the night and at the end of the day. The glucose content in µg glucose per g fresh-weight (FW) content corresponds to the starch content after the free glucose has been washed out of the leaf material and the remaining starch has been broken down to glucose with beta-glucosidase.

In both diagrams (figure 20 and 21) is shown that the transitory starch content, shown as Glucose content per gram fresh weight of the leaf sample, of all observed plant lines is higher at the end of the day compared to the end-of-the-night samples. The transitory starch content of 2-week-old seedlings per gram fresh-weight at the end of the day is overall a third compared to 4-week-old plants. The transitory starch content of 2-week-old seedlings per gram of fresh weight at the end of the day is about one third compared to the 4-week-old plants. Interestingly, this does not apply to the starch content at the end of the night. Here the absolute values per gram of fresh weight are about the same. This has an effect on the percentage of starch content at the end of the day and at the end of the night when comparing the 2-week-old seedlings with the 4-week-old plants. In the wild type, both the 2-week-old seedlings and the 4-week-old plants still have approx. 12.5 % of the plant's starch content remaining at the end of the night. In the 2-week-old seedlings double knockout and overexpression lines, approx. 20 % of the transitory starch is still left at the end of the night, whereas in the 4-week-old plants only approx. 6 % is left in both lines.

3.3.2 Discussion- Impact of OEF18 on transitory starch degradation

In this part the impact of OEF18 in the degradation of the transitory starch of chloroplasts has been observed. The results indicate that the overall design of the experiment has been

successful, as the OEF18-expressing plants retain only a fraction—between one-fifth and one-sixteenth—of the synthesized transitory starch at the end of the night compared to the end of the day under both growth conditions. This substantial reduction aligns with the hypothesis that OEF18 plays a role in starch metabolism. If the *oef18/oef18l* double knockout line significantly impacts transitory starch degradation, similar results to those observed by Dr. Przemyslaw Kmiecik (Figure 2) would be expected. Specifically, Kmiecik's findings show that the *oef18* single knockout and *oef18/oef18l* double knockout lines accumulated 60% and 70% of the synthesized transitory starch, respectively, by the end of the night. These observations suggest that OEF18 is involved in the regulation of starch degradation.

Interestingly, this role for OEF18 could parallel the mechanisms described by (Wang *et al.*, 2015), who reported the involvement of beta-tubulin-8 in a process known as starch excess (SEX) chlorophagy, which plays a specialized role in transitory starch degradation in *Nicotiana benthamiana* and potentially *Arabidopsis thaliana*. Wang and colleagues suggested that the microtubule cytoskeleton might influence starch degradation, either through direct or indirect interactions with SEX phenotype-generating factors. OEF18, which has been proposed as an interaction partner for tubulin-8 (Kmiecik, 2018), may function as an anchor protein, facilitating the interaction of tubulin with chloroplasts and thereby promoting starch degradation. In Chapter 3.2 the involvement of OEF18 in the stromule formation has been proven, which would give OEF18 an indirect role in starch degradation processes as SSGLs are exported via stromules out of the chloroplast.

However, the results from repeated experiments (Figures 20 and 21) show discrepancies when compared to the initial data (figure 2). In contrast to Figure 2, the *oef18/oef18l* double knockout line exhibited similar behavior to the OEF18 overexpression line regarding transitory starch degradation, regardless of plant aging conditions. This inconsistency raises questions about OEF18's involvement in starch degradation and suggests it may not be directly participating in SEX chlorophagy, as initially hypothesized. Since these repeated experiments were performed independently, it is unlikely that the deviations observed are artifacts. Therefore, these results challenge the previously assumed role of OEF18 in starch degradation and warrant further investigation into its precise function. To prevent high standard deviations for a possible recovery experiment ten instead of six leaves from different plant from the same line are suggested.

3.4 OEF18 as interaction partner of tubules

3.4.1 Results – OEF18 as interaction partner of tubules

Tubulins are suggested to be interacting proteins of OEF18, since β-tubulin-7 and β-tubulin-8 have been observed in a membrane Y2H screen. In an independent co-IP experiment against OEF18 tubulins 2-9 have been found as well. Since a microtubule binding protein spin-down assay has already been done by Dr. Przemyslaw Kmiecik with no results that could suggest an interaction of microtubules with OEF18, it could still be, that OEF18 is binding only at the very end of microtubules and act as an anchor protein like a linker between the organelle (peroxisome or chloroplast) and the microtubules. To clarify this a biased Y2H assay of OEF18 with tubulin2-tubulin 9 is assessed to cancel out possible false-positive or even false-negative interactions and prove a real interaction.

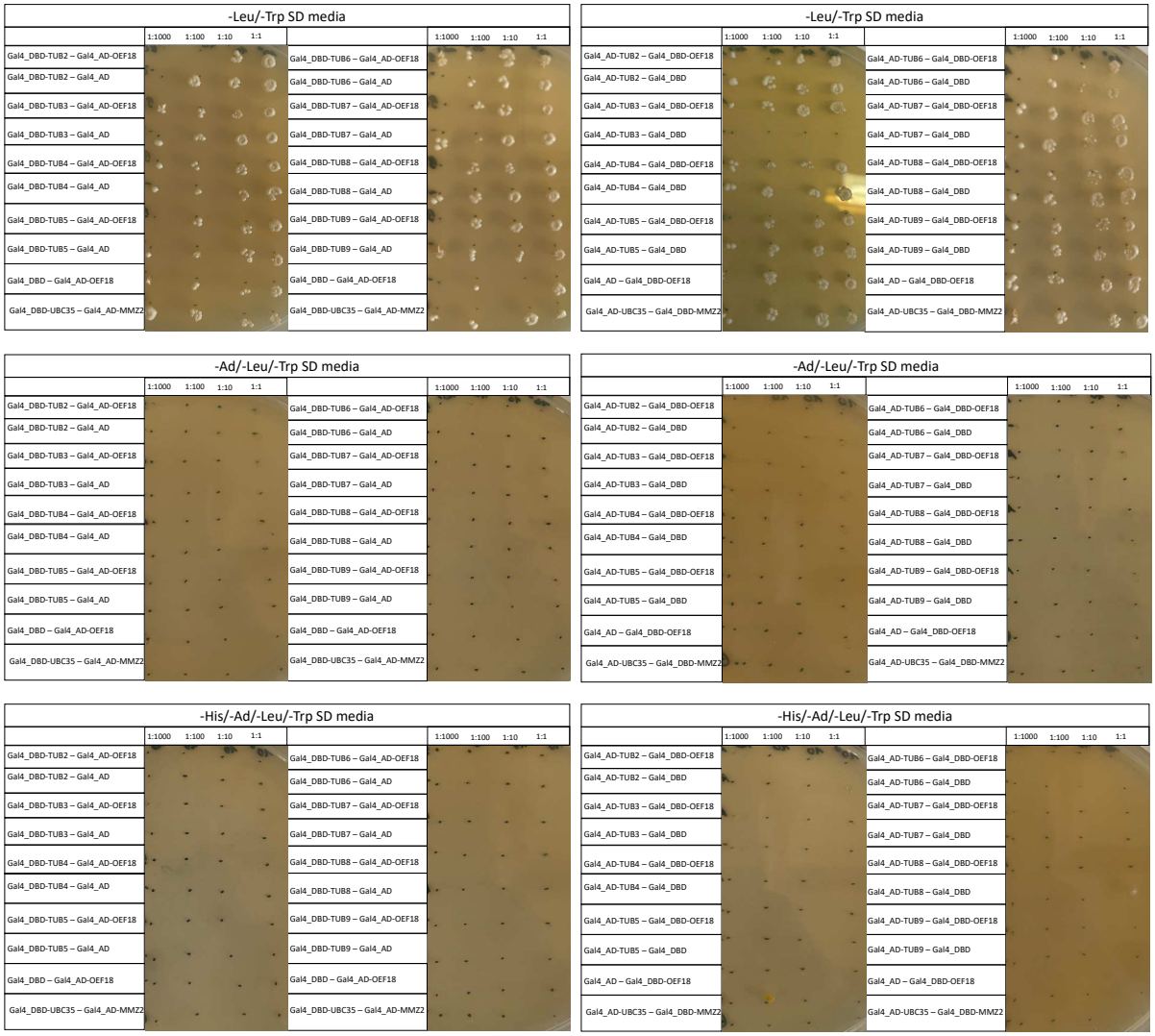

Figure 22: Yeast cells (*S. cerevisiae* from strain PJ69-4alpha) expressed Tubulin2 – Tubulin 9 or OEF18 in the activation domain vector pGAD424 and OEF18 or Tubulin2 – Tubulin 9 proteins fused to a GAL4 DNA binding domain. pGBKT7 is the empty vector (containing Trp1 gene), which was used for the expression of DNA binding domain (Gal4_DBD) fusions to TUB2 - TUB9 or OEF18. pGAD424 is the corresponding empty vector (containing Leu2 gene) which was used for the expression of GAL4 activation domain fusions to TUB2-TUB9 or OEF18. The yeast cells were spread out in dilutions 1:1, 1:10, 1:100, 1:1000. As a negative control one empty vector was transformed with proteins fused to Gal4 DNA binding domain or the GAL4 activation

domain. As a positive control UBC35/MMZ2 (Yin *et al.*, 2007) provided by Prof. Andreas Bachmair was used. Top left: TUB2-TUB9 fused to GAL4 DNA binding domain and OEF18 fused to GAL4 activation domain grown on -Leu/-Trp selective dropout media. Top right: OEF18 fused to GAL4 DNA binding domain and TUB2-TUB9 fused to GAL4 activation domain grown on -leucin (Leu)/-tryptophan (Trp) selective dropout media. Middle left: TUB2-TUB9 fused to GAL4 DNA binding domain and OEF18 fused to GAL4 activation domain grown on -adenin (Ade)/-Leu/-Trp selective dropout media. Middle right: OEF18 fused to GAL4 DNA binding domain and TUB2-TUB9 fused to GAL4 activation domain grown on -Ade/-Leu/-Trp selective dropout media. Bottom left: TUB2-TUB9 fused to GAL4 DNA binding domain and OEF18 fused to GAL4 activation domain grown on -histidin (His)/-Ade/-Leu/-Trp selective dropout media. Bottom right: OEF18 fused to GAL4 DNA binding domain and TUB2-TUB9 fused to GAL4 activation domain grown on -His/-Ade-Leu/-Trp selective dropout media.

The yeast cells have been grown on the -Leu/-Trp SD plates, showing that the bait construct as well as the prey construct have been successfully transformed into the yeast cells. This indicates that the constructs were taken up to the yeast cells and that the auxotrophic markers (TRP1 and LEU2) are functional in every transformed line, except the tubulin3 prey construt. No colonies were observed on the selective plates that require the activation of the HIS3 or the ADE2 reporter genes activated by the Alcohol dehydrogenase (ADH1) promoter. This means that a protein-protein interaction did not occur, or there is an issue with the activation of the reporter genes.

3.4.2 Discussion – OEF18 as interaction partner of tubules

In this experiment, the goal was to assess the interaction between a bait and prey construct using a yeast strain containing the HIS3 and ADE2 reporter genes. Both constructs were successfully transformed into the yeast cells, as evidenced by growth on -Leu/-Trp SD plates, indicating that the LEU2 and TRP1 selection markers were functional and that both bait and prey plasmids were present in the cells.

However, despite the presence of the bait and prey constructs, no growth was observed on the selective -Leu/-Trp/-His and -Leu/-Trp/-Ade SD plates, which are indicative of interaction-dependent activation of the HIS3 and ADE2 reporter genes. This result suggests that the interaction between the bait and prey proteins either did not occur or was not sufficient to activate the transcription of the reporter genes under the conditions tested. That could be due to various reasons:

The absence of growth on selective media suggests a potential problem with the activation of the HIS3 and ADE2 reporter genes. The fact that even a known positive control failed to grow under the same conditions indicates that the issue may not lie with the specific bait or prey constructs used. Instead, there could be problems with the integrity or functionality of the reporter genes in the yeast strain. Mutations or deletions in these loci could prevent proper

transcription, or the ADH1 promoter driving these reporter genes may not be functioning as expected under the experimental conditions. The ADH1 promoter is known for its robust expression in S. cerevisiae, making it unlikely that low protein expression levels are the cause of the negative results. Nevertheless, verifying protein expression through a method like Western blotting could further confirm this. The experiment was conducted with a range of cell densities (OD600 of 1, 0.1, 0.01, and 0.001), minimizing the likelihood that cell concentration was a limiting factor. Optimal growth conditions (30°C for 4 days) were maintained, suggesting that environmental factors were also not a primary issue. Given that plates were prepared independently on two separate occasions with consistent results, it is unlikely that plate composition or preparation error contributed to the lack of growth. Based on these considerations, it seems prudent to attempt the experiment using a different yeast strain or system e.g., yeast strain L40 using the LexA system, accompanied by a validated positive control. Ensuring that the positive control grows under the selective conditions will be critical for assessing the functionality of the assay. Once this is confirmed, the results can be re-evaluated to determine the presence or absence of protein-protein interactions in the test constructs.

4. Conclusion

The overarching goal of this study was to explore the biological function of the EF-hand protein OEF18, located in both the chloroplast outer envelope and peroxisomal membranes. Through multiple experimental approaches, it was aimed to determine OEF18's role in processes such as autophagy, stromule formation, starch degradation, and potential protein-protein interactions.

The findings of this thesis present OEF18 as a key player in certain cellular processes, though its role appears to be more selective than initially hypothesized. While OEF18 was not implicated in chloroplast degradation during stress responses, as evidenced by Imaging PAM results and growth assay under starvation and abiotic stresses, its involvement in stromule formation under normal conditions was clearly established. A reduction in stromule frequency in the *oef18/oef18l* double knockout lines highlights OEF18's positive influence on stromule dynamics under control conditions. Additionally, the role of calcium ions in stromule formation underscores the importance of OEF18 in cytoskeletal interactions, though further research is required to clarify its mechanism. The addition of sucrose also showed that different OEF18 independent pathways for stromule formation are present.

Unexpectedly, despite earlier indications, the role of OEF18 in starch degradation remains uncertain. The results of repeated experiments suggest that OEF18's influence on starch metabolism may not be as direct as previously thought, contradicting earlier observations. Finally, although no protein-protein interactions were observed in the Y2H assays, the issues with the reporter system call for a re-evaluation of this approach.

In summary, this thesis adds new insights into OEF18's role in stromule formation and points towards a more nuanced understanding of its involvement in chloroplast processes. Further studies will be essential to unravel its precise functions, particularly in relation to calcium signalling and cytoskeletal dynamics.

In response to the three bullet points outlined in the introduction, the findings can be summarized as:

1. **OEF18 is involved in the chloroplast stromule formation under control conditions**. Additionally, the absence of calcium ions showed a reduced stromule frequency.

2. **OEF18 does not show an involvement in chlorophagy processes**, as lack of evidence of phenotypes in knockout lines under autophagy inducing stress conditions. Its involvement in starch degradation was also disproved.
3. **The interaction of OEF18 with β-tubules remains unclear** due to an unfunctional positive control.

5. References

Akhmanova, A. and Steinmetz, M.O. (2008) Tracking the ends: a dynamic protein network controls the fate of microtubule tips. *Nat Rev Mol Cell Biol*, **9**, 309–322.

Anon (1989) A conserved tripeptide sorts proteins to peroxisomes. *J Cell Biol*, **108**, 1657–1664.

Avin-Wittenberg, T. (2018) Autophagy and its role in plant abiotic stress management. *Plant Cell & Environment*, **42**, 1045–1053.

Baker, N.R. (2008) Chlorophyll Fluorescence: A Probe of Photosynthesis In Vivo. *Annu. Rev. Plant Biol.*, **59**, 89–113.

Barbagallo, R.P., Oxborough, K., Pallett, K.E. and Baker, N.R. (2003) Rapid, Noninvasive Screening for Perturbations of Metabolism and Plant Growth Using Chlorophyll Fluorescence Imaging. *Plant Physiology*, **132**, 485–493.

Bassham, D.C. (2009) Function and regulation of macroautophagy in plants. *Biochimica et Biophysica Acta (BBA) - Molecular Cell Research*, **1793**, 1397–1403.

Bassham, D.C. (2007) Plant autophagy—more than a starvation response. *Current Opinion in Plant Biology*, **10**, 587–593.

Bassham, D.C., Laporte, M., Marty, F., Moriyasu, Y., Ohsumi, Y., Olsen, L.J. and Yoshimoto, K. (2006) Autophagy in Development and Stress Responses of Plants. *Autophagy*, **2**, 2–11.

Castro, E. de, Sigrist, C.J.A., Gattiker, A., Bulliard, V., Langendijk-Genevaux, P.S., Gasteiger, E., Bairoch, A. and Hulo, N. (2006) ScanProsite: detection of PROSITE signature matches and ProRule-associated functional and structural residues in proteins. *Nucleic Acids Research*, **34**, W362–W365.

Chanoca, A., Kovinich, N., Burkel, B., Stecha, S., Bohorquez-Restrepo, A., Ueda, T., Eliceiri, K.W., Grotewold, E. and Otegui, M.S. (2015) Anthocyanin Vacuolar Inclusions Form by a Microautophagy Mechanism. *Plant Cell*, **27**, 2545–2559.

Das, G., Shravage, B.V. and Baehrecke, E.H. (2012) Regulation and Function of Autophagy during Cell Survival and Cell Death. *Cold Spring Harb Perspect Biol*, **4**, a008813.

De Duve, C. and Wattiaux, R. (1966) Functions of Lysosomes. *Annu. Rev. Physiol.*, **28**, 435–492.

Díaz-Troya, S., Pérez-Pérez, M.E., Florencio, F.J. and Crespo, J.L. (2008) The role of TOR in autophagy regulation from yeast to plants and mammals. *Autophagy*, **4**, 851–865.

Ding, X., Zhang, X., Paez-Valencia, J., McLoughlin, F., Reyes, F.C., Morohashi, K., Grotewold, E., Vierstra, R.D. and Otegui, M.S. (2022) Microautophagy Mediates Vacuolar

Delivery of Storage Proteins in Maize Aleurone Cells. *Front. Plant Sci.*, **13**. Available at: https://www.frontiersin.org/journals/plant-science/articles/10.3389/fpls.2022.833612/full [Accessed October 10, 2024].

Dodd, A.N., Kudla, J. and Sanders, D. (2010) The Language of Calcium Signaling. *Annu. Rev. Plant Biol.*, **61**, 593–620.

Doelling, J.H., Walker, J.M., Friedman, E.M., Thompson, A.R. and Vierstra, R.D. (2002) The APG8/12-activating Enzyme APG7 Is Required for Proper Nutrient Recycling and Senescence in Arabidopsis thaliana. *Journal of Biological Chemistry*, **277**, 33105–33114.

Hanson, M.R. and Hines, K.M. (2018) Stromules: Probing Formation and Function. *Plant Physiol*, **176**, 128–137.

Haruta, N., Sumiyoshi, E., Honda, Y., Terasawa, M., Uchiyama, C., Toya, M., Kubota, Y. and Sugimoto, A. (2023) A germline-specific role for unconventional components of the γ-tubulin complex in Caenorhabditis elegans. *Journal of Cell Science*, **136**, jcs260922.

Hirokawa, N., Noda, Y., Tanaka, Y. and Niwa, S. (2009) Kinesin superfamily motor proteins and intracellular transport. *Nat Rev Mol Cell Biol*, **10**, 682–696.

Hörtensteiner, S. and Feller, U. (2002) Nitrogen metabolism and remobilization during senescence. *Journal of Experimental Botany*, **53**, 927–937.

Izumi, M. and Nakamura, S. (2018) Chloroplast Protein Turnover: The Influence of Extraplastidic Processes, Including Autophagy. *International Journal of Molecular Sciences*, **19**, 828.

Johansen, T. and Lamark, T. (2011) Selective autophagy mediated by autophagic adapter proteins. *Autophagy*, **7**, 279–296.

Kamada, Y., Funakoshi, T., Shintani, T., Nagano, K., Ohsumi, M. and Ohsumi, Y. (2000) Tor-Mediated Induction of Autophagy via an Apg1 Protein Kinase Complex. *The Journal of Cell Biology*, **150**, 1507–1513.

Kamranfar, I., Xue, G.-P., Tohge, T., Sedaghatmehr, M., Fernie, A.R., Balazadeh, S. and Mueller-Roeber, B. (2018) Transcription factor RD26 is a key regulator of metabolic reprogramming during dark-induced senescence. *New Phytologist*, **218**, 1543–1557.

Kelly, S.M., Jess, T.J. and Price, N.C. (2005) How to study proteins by circular dichroism. *Biochimica et Biophysica Acta (BBA) - Proteins and Proteomics*, **1751**, 119–139.

Ketelaar, T., Voss, C., Dimmock, S.A., Thumm, M. and Hussey, P.J. (2004) *Arabidopsis* homologues of the autophagy protein Atg8 are a novel family of microtubule binding proteins. *FEBS Letters*, **567**, 302–306.

Kihara, A., Noda, T., Ishihara, N. and Ohsumi, Y. (2001) Two Distinct Vps34

Phosphatidylinositol 3–Kinase Complexes Function in Autophagy and Carboxypeptidase Y Sorting inSaccharomyces cerevisiae. *Journal of Cell Biology*, **152**, 519–530.

Kikuchi, Y., Nakamura, S., Woodson, J.D., Ishida, H., Ling, Q., Hidema, J., Jarvis, R.P., Hagihara, S. and Izumi, M. (2020) Chloroplast Autophagy and Ubiquitination Combine to Manage Oxidative Damage and Starvation Responses. *Plant Physiol.*, **183**, 1531–1544.

Kmiecik, P. (2018) *Biochemical and functional characterization of OEF18 a novel calcium binding protein located in peroxisomes and chloroplasts.* Vienna: University of Vienna.

Köchl, R., Hu, X.W., Chan, E.Y.W. and Tooze, S.A. (2006) Microtubules Facilitate Autophagosome Formation and Fusion of Autophagosomes with Endosomes. *Traffic*, **7**, 129–145.

Kumar, A.S., Park, E., Nedo, A., et al. (2018) Stromule extension along microtubules coordinated with actin-mediated anchoring guides perinuclear chloroplast movement during innate immunity J. T. Greenberg, ed. *eLife*, **7**, e23625.

Ling, Q. and Jarvis, P. (2016) Plant Signaling: Ubiquitin Pulls the Trigger on Chloroplast Degradation. *Current Biology*, **26**, R38–R40.

Ling, Q. and Jarvis, P. (2015) Regulation of Chloroplast Protein Import by the Ubiquitin E3 Ligase SP1 Is Important for Stress Tolerance in Plants. *Current Biology*, **25**, 2527–2534.

Liu, X., Wang, Y., Yu, L., Tong, Z., Chen, L., Liu, H. and Li, X. (2013) Thermal degradation and stability of starch under different processing conditions. *Starch - Stärke*, **65**, 48–60.

Liu, Y. and Bassham, D.C. (2012) Autophagy: Pathways for Self-Eating in Plant Cells. *Annu. Rev. Plant Biol.*, **63**, 215–237.

Ma, C. and Reumann, S. (2008) Improved prediction of peroxisomal PTS1 proteins from genome sequences based on experimental subcellular targeting analyses as exemplified for protein kinases from Arabidopsis. *Journal of Experimental Botany*, **59**, 3767–3779.

Mackeh, R., Perdiz, D., Lorin, S., Codogno, P. and Poüs, C. (2013) Autophagy and microtubules – new story, old players. *Journal of Cell Science*, **126**, 1071–1080.

Malinova, I., Qasim, H.M., Brust, H. and Fettke, J. (2018) Parameters of Starch Granule Genesis in Chloroplasts of Arabidopsis thaliana. *Front. Plant Sci.*, **9**. Available at: https://www.frontiersin.org/journals/plant-science/articles/10.3389/fpls.2018.00761/full [Accessed October 7, 2024].

Maxwell, K. and Johnson, G.N. (2000) Chlorophyll fluorescence—a practical guide. *Journal of Experimental Botany*, **51**, 659–668.

McIntosh, J.R., Volkov, V., Ataullakhanov, F.I. and Grishchuk, E.L. (2010) Tubulin

depolymerization may be an ancient biological motor. *Journal of Cell Science*, **123**, 3425–3434.

Michaeli, S., Galili, G., Genschik, P., Fernie, A.R. and Avin-Wittenberg, T. (2016) Autophagy in Plants – What's New on the Menu? *Trends in Plant Science*, **21**, 134–144.

Michaeli, S., Honig, A., Levanony, H., Peled-Zehavi, H. and Galili, G. (2014) *Arabidopsis* ATG8-INTERACTING PROTEIN1 Is Involved in Autophagy-Dependent Vesicular Trafficking of Plastid Proteins to the Vacuole. *The Plant Cell*, **26**, 4084–4101.

Mizushima, N. and Komatsu, M. (2011) Autophagy: Renovation of Cells and Tissues. *Cell*, **147**, 728–741.

Nakamura, S., Hidema, J., Sakamoto, W., Ishida, H. and Izumi, M. (2018) Selective Elimination of Membrane-Damaged Chloroplasts via Microautophagy. *Plant Physiol.*, **177**, 1007–1026.

Nakamura, S. and Izumi, M. (2019) Chlorophagy is ATG gene-dependent microautophagy process. *Plant Signaling & Behavior*, **14**, 1554469.

Nakamura, S. and Izumi, M. (2018) Regulation of Chlorophagy during Photoinhibition and Senescence: Lessons from Mitophagy. *Plant and Cell Physiology*, **59**, 1135–1143.

Nogales, E., Wolf, S.G. and Downing, K.H. (1998) Erratum: Structure of the αβ tubulin dimer by electron crystallography. *Nature*, **393**, 191–191.

Ohsumi, Y. (2014) Historical landmarks of autophagy research. *Cell Res*, **24**, 9–23.

Oikawa, K., Goto-Yamada, S., Hayashi, Y., et al. (2022) Pexophagy suppresses ROS-induced damage in leaf cells under high-intensity light. *Nat Commun*, **13**, 7493.

Orenstein, S.J. and Cuervo, A.M. (2010) Chaperone-mediated autophagy: Molecular mechanisms and physiological relevance. *Seminars in Cell & Developmental Biology*, **21**, 719–726.

Radivojac, P., Vacic, V., Haynes, C., Cocklin, R.R., Mohan, A., Heyen, J.W., Goebl, M.G. and Iakoucheva, L.M. (2010) Identification, analysis, and prediction of protein ubiquitination sites. *Proteins: Structure, Function, and Bioinformatics*, **78**, 365–380.

Romanov, J., Walczak, M., Ibiricu, I., Schüchner, S., Ogris, E., Kraft, C. and Martens, S. (2012) Mechanism and functions of membrane binding by the Atg5-Atg12/Atg16 complex during autophagosome formation: Role of Atg5-Atg12/Atg16 during autophagy. *The EMBO Journal*, **31**, 4304–4317.

Romero-Barrios, N. and Vert, G. (2018) Proteasome-independent functions of lysine-63 polyubiquitination in plants. *New Phytologist*, **217**, 995–1011.

Schattat, M. and Klösgen, R. (2011) Induction of stromule formation by extracellular

sucrose and glucose in epidermal leaf tissue of Arabidopsis thaliana. *BMC Plant Biol*, **11**, 115.

Siegrist, S.E. and Doe, C.Q. (2007) Microtubule-induced cortical cell polarity. *Genes Dev.*, **21**, 483–496.

Sieńko, K., Poormassalehgoo, A., Yamada, K. and Goto-Yamada, S. (2020) Microautophagy in Plants: Consideration of Its Molecular Mechanism. *Cells*, **9**, 887.

Soto-Burgos, J., Zhuang, X., Jiang, L. and Bassham, D.C. (2018) Dynamics of Autophagosome Formation. *Plant Physiology*, **176**, 219–229.

Stael, S., Wurzinger, B., Mair, A., Mehlmer, N., Vothknecht, U.C. and Teige, M. (2012) Plant organellar calcium signalling: an emerging field. *Journal of Experimental Botany*, **63**, 1525–1542.

Su, T., Li, X., Yang, M., Shao, Q., Zhao, Y., Ma, C. and Wang, P. (2020) Autophagy: An Intracellular Degradation Pathway Regulating Plant Survival and Stress Response. *Front. Plant Sci.*, **11**, 164.

Svenning, S., Lamark, T., Krause, K. and Johansen, T. (2011) Plant NBR1 is a selective autophagy substrate and a functional hybrid of the mammalian autophagic adapters NBR1 and p62/SQSTM1. *Autophagy*, **7**, 993–1010.

Van Doorn, W.G. and Woltering, E.J. (2005) Many ways to exit? Cell death categories in plants. *Trends in Plant Science*, **10**, 117–122.

Veljanovski, V. and Batoko, H. (2014) Selective autophagy of non-ubiquitylated targets in plants: looking for cognate receptor/adaptor proteins. *Front. Plant Sci.*, **5**. Available at: https://www.frontiersin.org/journals/plant-science/articles/10.3389/fpls.2014.00308/full [Accessed October 10, 2024].

Wang, P., Wang, T., Han, J., Li, M., Zhao, Y., Su, T. and Ma, C. (2021) Plant Autophagy: An Intricate Process Controlled by Various Signaling Pathways. *Front. Plant Sci.*, **12**. Available at: https://www.frontiersin.org/journals/plant-science/articles/10.3389/fpls.2021.754982/full [Accessed October 17, 2024].

Wang, S. and Blumwald, E. (2014) Stress-Induced Chloroplast Degradation in *Arabidopsis* Is Regulated via a Process Independent of Autophagy and Senescence-Associated Vacuoles. *Plant Cell*, **26**, 4875–4888.

Wang, Y., Yu, B., Zhao, J., et al. (2013) Autophagy Contributes to Leaf Starch Degradation. *The Plant Cell*, **25**, 1383–1399.

Wang, Y., Zheng, X. and Liu, Y. (2016) Functional links between microtubules, autophagy and leaf starch degradation in plants. *Plant Signaling & Behavior*, **11**, e1201626.

Wang, Y., Zheng, X., Yu, B., et al. (2015) Disruption of microtubules in plants suppresses macroautophagy and triggers starch excess-associated chloroplast autophagy. *Autophagy*, **11**, 2259–2274.

Woodson, J.D., Matthew S. Joens, Andrew B. Sinson, Jonathan Gilkerson, Patrice A. Salomé, Detlef Weigel, James A. Fitzpatrick, and Joanne Chory (2015) Ubiquitin facilitates a quality-control pathway that removes damaged chloroplasts. *Science*, 450–454.

Yagyu, M. and Yoshimoto, K. (2024) New insights into plant autophagy: molecular mechanisms and roles in development and stress responses D. Ort, ed. *Journal of Experimental Botany*, **75**, 1234–1251.

Yin, X.-J., Volk, S., Ljung, K., et al. (2007) Ubiquitin Lysine 63 Chain–Forming Ligases Regulate Apical Dominance in *Arabidopsis*. *The Plant Cell*, **19**, 1898–1911.

Yoshitake, Y., Nakamura, S., Shinozaki, D., Izumi, M., Yoshimoto, K., Ohta, H. and Shimojima, M. (2021) RCB-mediated chlorophagy caused by oversupply of nitrogen suppresses phosphate-starvation stress in plants. *Plant Physiology*, **185**, 318–330.

Zaffagnini, G. and Martens, S. (2016) Mechanisms of Selective Autophagy. *Journal of Molecular Biology*, **428**, 1714–1724.

Zeng, W., Wang, M., Zhang, Y., Zhou, T. and Zong, Z. (2024) Targeting mitochondrial damage: shining a new light on immunotherapy. *Front. Immunol.*, **15**. Available at: https://www.frontiersin.org/journals/immunology/articles/10.3389/fimmu.2024.1432633/full [Accessed October 10, 2024].

Zhang, K. and Gan, S.-S. (2012) An Abscisic Acid-AtNAP Transcription Factor-SAG113 Protein Phosphatase 2C Regulatory Chain for Controlling Dehydration in Senescing Arabidopsis Leaves. *Plant Physiology*, **158**, 961–969.

Zhang, X., Ding, X., Marshall, R.S., Paez-Valencia, J., Lacey, P., Vierstra, R.D. and Otegui, M.S. (2020) Reticulon proteins modulate autophagy of the endoplasmic reticulum in maize endosperm. *eLife*, **9**, e51918.

Zheng, Y., Wong, M.L. and Alberts, B. (1995) Nucleation of microtubule assembly by a y-tubulin-containing ring complex. , **378**.

Zhuang, X., Chung, K.P. and Jiang, L. (2016) Origin of the Autophagosomal Membrane in Plants. *Front. Plant Sci.*, **7**. Available at: https://www.frontiersin.org/journals/plant-science/articles/10.3389/fpls.2016.01655/full [Accessed October 10, 2024].

Zhuang, X. and Jiang, L. (2019) Chloroplast Degradation: Multiple Routes Into the Vacuole. *Front. Plant Sci.*, **10**, 359.

Zientara-Rytter, K. and Sirko, A. (2014) Selective autophagy receptor Joka2 co-localizes

with cytoskeleton in plant cells. *Plant Signaling & Behavior*, **9**, e28523.